R. & M. No. 2749
(13,162, 14,217)
A.R.C. Technical Report

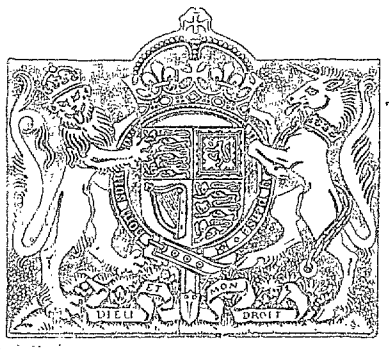



MINISTRY OF SUPPLY

AERONAUTICAL RESEARCH COUNCIL
REPORTS AND MEMORANDA

# Aerodynamic Forces on Biconvex Aerofoils Oscillating in a Supersonic Airstream

*By*
W. P. Jones, M.A. and Sylvia W. Skan,
of the Aerodynamics Division, N.P.L.

---

# Effect of Thickness on the Aerodynamic Forces on Biconvex Aerofoils Oscillating in a Supersonic Airstream, and Calculation of Forces for Aerofoil with Flap

*By*
Sylvia W. Skan,
of the Aerodynamics Division, N.P.L.



LONDON: HER MAJESTY'S STATIONERY OFFICE
1953
NINE SHILLINGS NET

# Aerodynamic Forces on Biconvex Aerofoils Oscillating in a Supersonic Airstream*

*By*

W. P. Jones, M.A. and Sylvia W. Skan,
of the Aerodynamics Division, N.P.L.



*Reports and Memoranda No.* 2749
*August,* 1951

*Summary.*—A method for the calculation of the aerodynamic forces on an oscillating aerofoil which allows for the effect of thickness is developed. The steady flow regime for zero or mean incidence is first determined for isentropic, irrotational and inviscid flow conditions. A small disturbance is then assumed and the non-linear equation defining the subsequent motion is reduced to a linear equation for the velocity potential of the disturbance. This is expressed in difference form and solved numerically by a step-by-step process. The results obtained show good agreement with the known solutions for a thick aerofoil at incidence in steady flow, and for the case of an oscillating flat plate. Consequently, it is believed that the results derived for an oscillating biconvex aerofoil are reasonably accurate.

Aerodynamic lift and pitching moment derivatives for a 5 per cent thick, symmetrical, circular-arc aerofoil at Mach numbers $M = 1{\cdot}4$, $1{\cdot}5$ and $2{\cdot}0$ are given for a range of frequencies and compared with values obtained on the basis of the flat plate theory. The effect of thickness appears to be important at the lower values of $M$, and the results indicate that the flat plate theory is not sufficiently accurate.

1. *Introduction.*—Measurements of the aerodynamic forces on an oscillating aerofoil[1] indicate that the linearised flat plate theory for the calculation of such forces is inadequate. This is not surprising as it is known that even in steady motion the simple Ackeret theory, which neglects the effect of thickness, is unreliable when chordwise lift distributions are required. Busemann's second-order theory[2], however, gives better agreement with experiment, and the object of this paper is to develop a method which will give the same degree of accuracy for solutions of oscillatory problems.

The method suggested is tried out for a biconvex aerofoil describing pitching and translational oscillations. A thickness/chord ratio of $0{\cdot}05$ is assumed, and derivatives are calculated for a range of Mach numbers and frequencies for comparison with results based on the flat plate theory. As shown in Figs. 5 and 6, the chordwise lift distributions differ considerably, and it appears that in the calculation of flutter derivatives allowance should be made for effects due to the shape of the aerofoil.

Wind tunnel tests to check the accuracy of the present theory are to be made shortly at the National Physical Laboratory. The experimental information obtained should provide much useful data for possible further theoretical development. However, if the effects due to the boundary layer and the leading-edge shock wave are negligible, the present theory should give agreement with experiment.

Attempts to investigate the effect of viscosity could be made by assuming the aerofoil section to be thickened so as to include the boundary layer. This approach presupposes that the boundary-layer thickness is independent of time, and any results obtained on this basis would presumably be valid only for slow oscillations of infinitesimal amplitude.

* Published with the permission of the Director, National Physical Laboratory.
A.R.C. Report No. 13,162. May, 1950.



(52568) A

If the effect of the shock wave at the nose is to be included the flow can no longer be regarded as irrotational and isentropic. In principle, however, if the local values of $q_s$, $\theta_s$, $\mu_s$ could be determined everywhere, and if the correct boundary conditions could be established, the numerical technique used in this report could be applied.

For the particular aerofoil considered the assumption that the flow is isentropic and irrotational should be approximately valid in view of the low value of the thickness/chord ratio, namely 5 per cent, which corresponds to a wedge angle of about 12 deg. Experiment has shown that for aerofoils of this order of thickness Busemann's second-order theory gives good accuracy in the steady case[2]. In view of this evidence it is considered that the results given by the present method for the unsteady case are reasonably accurate. They should certainly be an improvement on those given by flat plate theory.

Further calculations for biconvex circular-arc, symmetrical aerofoils of various thickness/chord ratios are proposed for suitable ranges of Mach number and frequency parameter to provide complete sets of derivative coefficients corresponding to translational and pitching oscillations of the aerofoils. The method can also be used to determine control surface derivatives when the angular displacements are small.

2. *Equations of Motion.*—For isentropic, irrotational and inviscid flow in two-dimensions, the equations of motion are

$$\frac{d\tilde{u}}{dt} = -\frac{1}{\tilde{\rho}}\frac{\partial \tilde{p}}{\partial x}, \quad \frac{d\tilde{v}}{dt} = -\frac{1}{\tilde{\rho}}\frac{\partial \tilde{p}}{\partial y}, \qquad \text{(1)}$$

where $\frac{d}{dt} \equiv \frac{\partial}{\partial t} + \tilde{u}\frac{\partial}{\partial x} + \tilde{v}\frac{\partial}{\partial y}$ and $\tilde{u}$, $\tilde{v}$ denote the velocity components parallel to the $x$ and $y$ axes respectively. Since the flow is assumed to be isentropic, the pressure $\tilde{p}$ and the density $\tilde{\rho}$ satisfy the usual relation

$$\tilde{p} = k\tilde{\rho}^{\gamma}, \qquad \text{(2)}$$

where $k$ and $\gamma$ are constants.

The equation of continuity yields

$$\frac{dP}{dt} + \tilde{a}^2\left(\frac{\partial \tilde{u}}{\partial x} + \frac{\partial \tilde{v}}{\partial y}\right) = 0, \qquad \text{(3)}$$

where $P \equiv \int_{p_0}^{\tilde{p}} \frac{d\tilde{p}}{\tilde{\rho}}$ and $\tilde{a}$ $(\equiv \gamma p/\rho)$ denotes the local velocity of sound. For irrotational flow, the following relation is also valid, namely,

$$\frac{\partial \tilde{u}}{\partial y} = \frac{\partial \tilde{v}}{\partial x}. \qquad \text{(4)}$$

From the above equations it follows that

$$(\tilde{a}^2 - \tilde{u}^2)\frac{\partial \tilde{u}}{\partial x} - 2\tilde{u}\tilde{v}\frac{\partial \tilde{u}}{\partial y} + (\tilde{a}^2 - \tilde{v}^2)\frac{\partial \tilde{v}}{\partial y} = \frac{\partial^2 \tilde{\phi}}{\partial t^2} + \frac{\partial \tilde{q}^2}{\partial t}, \qquad \text{(5)}$$

and that

$$\frac{\tilde{a}^2}{\gamma - 1} + \frac{\partial \tilde{\phi}}{\partial t} + \frac{\tilde{q}^2}{2} = \text{const.}, \qquad \text{(6)}$$

where $\tilde{q}^2 \equiv \tilde{u}^2 + \tilde{v}^2$ and $\tilde{\phi}$ is the velocity potential. In polar co-ordinates $r$, $\Psi$, equation (5) yields

$$(\tilde{a}^2 - \tilde{v}^2)\frac{\partial \tilde{v}}{\partial r} + \frac{(\tilde{a}^2 - \tilde{u}^2)}{r}\frac{\partial \tilde{u}}{\partial \Psi} - \tilde{u}\tilde{v}\left(\frac{\partial \tilde{u}}{\partial r} + \frac{1}{r}\frac{\partial \tilde{v}}{\partial \Psi}\right) + \frac{\tilde{a}^2\tilde{v}}{r} = \frac{\partial^2 \tilde{\phi}}{\partial t^2} + \frac{\partial \tilde{q}^2}{\partial t} \quad .. \quad (7)$$

where $\tilde{u}$, $\tilde{v}$ now represent $\frac{1}{r}\frac{\partial \tilde{\phi}}{\partial \Psi}$ and $\frac{\partial \tilde{\phi}}{\partial r}$ respectively.

3. *Linearisation.*—It can be assumed that the flow around an infinitely thin flat plate at zero incidence is constant everywhere. If this flow is disturbed slightly the subsequent components of the velocity and the local speed of sound may be expressed as

$$\tilde{u} = U_s + u\,, \qquad \tilde{v} = v\,, \qquad \tilde{a} = a_s + a\,,$$

where $U_s$ is the constant velocity of the undisturbed stream*. Substitution in (5) and omission of second-order terms then yields the standard equation

$$(a_s^2 - U_s^2)\frac{\partial^2 \phi}{\partial x^2} + a_s^2\frac{\partial^2 \phi}{\partial y^2} = \frac{\partial^2 \phi}{\partial t^2} + 2U_s\frac{\partial^2 \phi}{\partial x\,\partial t}\,, \quad .. \quad .. \quad .. \quad .. \quad .. \quad (8)$$

where $\phi$ is the velocity potential of the disturbance. The solution of this equation is readily derived and will not be discussed in detail in this report (R. & M. 2140[3] and 2655[4]).

In the more general case of a thick aerofoil, linearisation leads to a more complicated equation than (8). For a biconvex circular-arc profile, which is the particular case considered in this note, the appropriate equation can be expressed most conveniently in terms of polar co-ordinates.

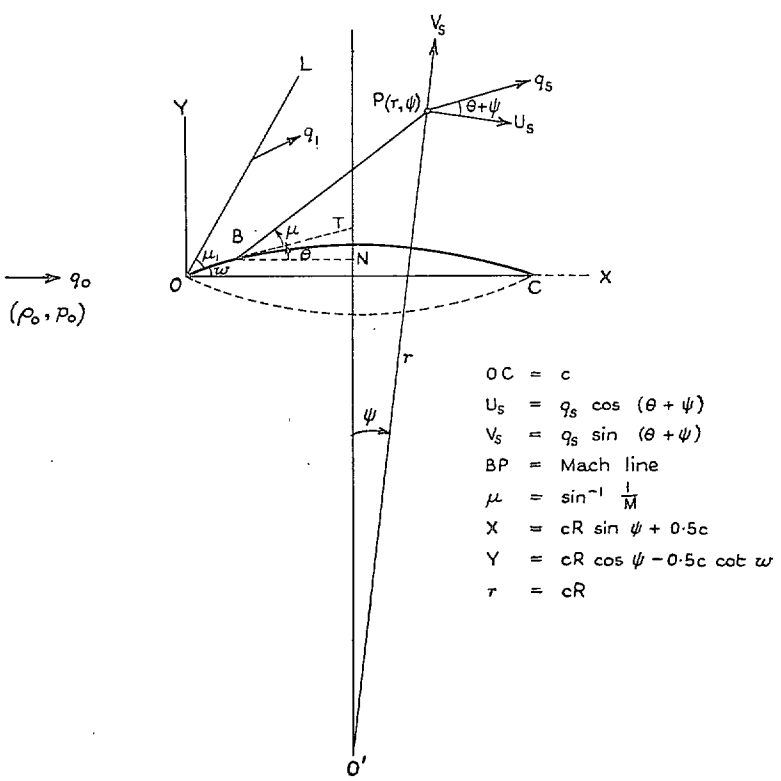


FIG. 1.

* The suffix $s$ denotes steady flow at zero incidence.



(52568) A 2

If the flow regime at zero incidence is specified by $U_s$, $V_s$ as shown above with corresponding fields of pressure and density, then by writing $\tilde{u} = U_s + u$, $\tilde{v} = V_s + v$, and $\tilde{a} = a_s + a$, and substituting in (7), the following linear equation can be derived for the disturbed flow, namely,

$$\left.\begin{aligned}&(a_s^2 - V_s^2)\frac{\partial v}{\partial r} + \frac{a_s^2 - U_s^2}{r}\frac{\partial u}{\partial \Psi} + \frac{v}{r}(a_s^2 - \gamma q_s^2 + V_s^2) - 2U_s V_s \frac{\partial u}{\partial r}\\ &- \frac{(\gamma+1)}{2}\left(\frac{u}{r}\frac{\partial}{\partial \Psi} + v\frac{\partial}{\partial r}\right)q_s^2 - (\gamma - 1)\,U_s^2\left(u\frac{\partial}{\partial r} - \frac{v}{r}\frac{\partial}{\partial \Psi}\right)\left(\frac{V_s}{U_s}\right)\\ &= \frac{\partial^2\phi}{\partial t^2} + 2U_s\frac{\partial u}{\partial t} + 2V_s\frac{\partial v}{\partial t} + \frac{\gamma - 1}{2a_s^2}\frac{\partial \phi}{\partial t}\left(\frac{U_s}{r}\frac{\partial}{\partial \Psi} + V_s\frac{\partial}{\partial r}\right)q_s^2 .\end{aligned}\right\} \quad .. \quad .. \quad (9)$$

In the above equation, $\phi$ represents the velocity potential of the disturbance ; $U_s$, $V_s$ are the known velocity components for steady flow at zero incidence; and $u$, $v$ denote $\frac{1}{r}\frac{\partial \phi}{\partial \Psi}$, $\frac{\partial \phi}{\partial r}$ respectively. For thin aerofoils $\theta$ is small, and for points in the neighbourhood of the aerofoil $\Psi$ is also small (*see* Fig. 1). At the surface of the aerofoil $\theta + \Psi = 0$ and $V_s$ is zero. It may therefore be assumed that

$$U_s = q_s , \qquad V_s = q_s(\theta + \Psi) \quad .. \quad .. \quad .. \quad .. \quad .. \quad .. \quad .. \quad .. \quad (10)$$

to a reasonable degree of accuracy. Since $V_s = 0$ at the surface, and since it is small elsewhere, it is assumed further that terms involving $V_s$ as a factor can be neglected. Equation (9) then reduces to

$$\begin{aligned}&a_s^2\frac{\partial v}{\partial r} + \frac{a_s^2 - q_s^2}{r}\frac{\partial u}{\partial \Psi} + \frac{v}{r}(a_s^2 - \gamma q_s^2) - \frac{\gamma+1}{2}\left(\frac{u}{r}\frac{\partial}{\partial \Psi} + v\frac{\partial}{\partial r}\right)q_s^2\\ &- (\gamma - 1)\,q_s^2\left(u\frac{\partial}{\partial r} - \frac{v}{r}\frac{\partial}{\partial \Psi}\right)(\theta + \Psi)\\ &= \frac{\partial^2\phi}{\partial t^2} + 2q_s\frac{\partial u}{\partial t} + \frac{\gamma - 1}{r}\frac{\partial \phi}{\partial t}\left(\frac{q_s}{a_s}\right)^2\frac{\partial q_s}{\partial \Psi}\end{aligned} \quad .. \quad .. \quad .. \quad .. \quad .. \quad .. \quad (11)$$

Since $u \equiv \frac{1}{r}\frac{\partial \phi}{\partial \Psi}$, $v \equiv \frac{\partial \phi}{\partial r}$, the above equation then leads directly to the following linear equation for $\phi$, namely,

$$\begin{aligned}&a_s^2\frac{\partial^2\phi}{\partial r^2} + \frac{a_s^2 - q_s^2}{r^2}\frac{\partial^2\phi}{\partial \Psi^2} + \frac{a_s^2 - q_s^2}{r}\frac{\partial \phi}{\partial r} - \frac{(\gamma+1)}{2}\left[\frac{1}{r^2}\frac{\partial q_s^2}{\partial \Psi}\frac{\partial \phi}{\partial \Psi} + \frac{\partial q_s^2}{\partial r}\frac{\partial \phi}{\partial r}\right]\\ &- \frac{(\gamma - 1)}{r}q_s^2\left(\frac{\partial \theta}{\partial r}\frac{\partial \phi}{\partial \Psi} - \frac{\partial \theta}{\partial \Psi}\frac{\partial \phi}{\partial r}\right)\\ &= \frac{\partial^2\phi}{\partial t^2} + \frac{2q_s}{r}\frac{\partial^2\phi}{\partial \Psi\,\partial t} + \frac{\gamma - 1}{r}\frac{\partial \phi}{\partial t}\left(\frac{q_s}{a_s}\right)^2\frac{\partial q_s}{\partial \Psi}.\end{aligned} \quad .. \quad .. \quad .. \quad .. \quad .. \quad .. \quad (12)$$

When the motion is steady the right-hand side of (12) vanishes, and the solution of the resulting equation with the boundary conditions appropriate to the case of an aerofoil at incidence should agree with the known exact solution for isentropic conditions. Equation (12) also reduces to (8) when the thickness of the aerofoil tends to zero. In general, however, the coefficients in (12) are variable and an analytical solution cannot readily be determined. The coefficients could be represented approximately as simple functions of $r$ and $\Psi$ and an attempt at such a solution could be made, but for the particular aerofoil considered in this report a numerical method of solution is developed.

The aerofoil is assumed to be describing simple harmonic oscillations of small amplitude with frequency $p/2\pi$ in the pitching and vertical translation degrees of freedom. For convenience in the subsequent analysis $\phi$ is replaced by $\Phi e^{ipt}$, where $\Phi$ represents the amplitude of the velocity potential of the disturbance. Substitution in (12) and omission of the exponential factor then leads to an equation of the form

$$A_0 \frac{\partial^2 \Phi}{\partial R^2} + \frac{A_1}{R^2} \frac{\partial^2 \Phi}{\partial \Psi^2} + A_2 \frac{\partial \Phi}{\partial R} + \frac{A_3}{R} \frac{\partial \Phi}{\partial \Psi} = \Phi (\lambda_0^2 B_0 + i\lambda_0 B_1) + \frac{i\lambda_0 B_2}{R} \frac{\partial \Phi}{\partial \Psi}, \quad .. \quad .. \quad (13)$$

where $R \equiv r/c$, $\lambda_0 \equiv pc/q_0$, and

$$\left.\begin{aligned}
A_0 &\equiv a_s^2/q_1^2 \\
A_1 &\equiv (a_s^2 - q_s^2)/q_1^2 \\
A_2 &\equiv \frac{a_s^2 - q_s^2}{R\, q_1^2} - \frac{\gamma + 1}{2} \frac{\partial}{\partial R} \left(\frac{q_s}{q_1}\right)^2 + \frac{(\gamma - 1)}{R} \left(\frac{q_s}{q_1}\right)^2 \frac{\partial \theta}{\partial \Psi} \\
A_3 &\equiv -\frac{\gamma + 1}{2R} \frac{\partial}{\partial \Psi} \left(\frac{q_s}{q_1}\right)^2 - (\gamma - 1) \left(\frac{q_s}{q_1}\right)^2 \frac{\partial \theta}{\partial R} \\
B_0 &\equiv -q_0^2/q_1^2 \\
B_1 &\equiv \frac{(\gamma - 1)}{R} \left(\frac{q_0}{q_1}\right) \left(\frac{q_s}{a_s}\right)^2 \frac{\partial}{\partial \Psi} \left(\frac{q_s}{q_1}\right) \\
B_2 &\equiv 2q_0 q_s/q_1^2 .
\end{aligned}\right\} \quad .. \quad .. \quad .. \quad (14)$$

The above coefficients are all determined by the flow past the aerofoil in its undisturbed position. When the aerofoil is oscillating about a mean incidence which is not zero, however, the coefficients are different according as to whether the flow above or below the aerofoil is considered. Hence, in general, the supersonic flow solutions would be determined by two forms of (13) which would refer to each side of the aerofoil respectively.

4. *Determination of the Coefficients.*—For the case considered in this paper, the aerofoil is assumed to be symmetrical and to be oscillating about the zero incidence position. Hence the undisturbed flow about the aerofoil in its mean position is symmetrical and the coefficients $A_0$, $B_0$, etc., will be the same at corresponding points above and below the aerofoil. It will be seen from (14) that these coefficients will be determined over the region of flow under consideration when the undisturbed velocity $q_s$ and its direction $\theta$ are known everywhere. Let us suppose that the values of $A_0$, $B_0$, etc., at P in Fig. 1 are required. At points along the characteristic line BP the flow is constant in magnitude and direction and is therefore determined when the flow at B on the boundary is known. The direction of flow is parallel to the tangent to the aerofoil surface at B, and $q_s$ is a function of $\theta$ ($\equiv\angle$ TBN) and the local Mach angle $\mu$ ($\equiv\angle$ PBT) as defined by the known relation[5].

$$\frac{1}{q} \frac{dq}{d\theta} = -\tan \mu . \quad .. \quad .. \quad .. \quad .. \quad .. \quad .. \quad .. \quad .. \quad (15)$$

When $w$ is small, the value of $\mu$ at B is given in terms of the deflection $\theta$ and the Mach angle $\mu_0$ of the undisturbed flow by

$$\theta = f(\mu) - f(\mu_0) , \quad .. \quad .. \quad .. \quad .. \quad .. \quad .. \quad .. \quad .. \quad (16)$$

where $$f(\mu) \equiv \left(\frac{\gamma + 1}{\gamma - 1}\right)^{1/2} \tan^{-1} \left\{ \left(\frac{\gamma + 1}{\gamma - 1}\right)^{1/2} \tan \mu \right\} - \mu .$$

In addition, for steady motion,

$$\frac{\tilde{a}^2}{\gamma - 1} + \frac{\tilde{q}^2}{2} = \frac{\tilde{a}_0^2}{\gamma - 1} + \frac{\tilde{q}_0^2}{2} = \text{constant}, \quad .. \quad .. \quad .. \quad .. \quad (17)$$

where $\tilde{a} \equiv \tilde{q} \sin \mu$. Hence,

$$\frac{\tilde{q}}{q_0} = \left(\frac{\gamma - 1 + 2 \sin^2 \mu_0}{\gamma - 1 + 2 \sin^2 \mu}\right)^{1/2}, \quad .. \quad .. \quad .. \quad .. \quad .. \quad .. \quad (18)$$

which gives $\tilde{q}$ when $\mu$ has been derived from (16). Before the above equations can be used, however, the point B must be determined such that BP is a characteristic line. Let $X_0$, $Y_0$ and $X$, $Y$ be the co-ordinates of B and P respectively, where $X$ and $Y$ are known and where $Y_0$ is a function of $X_0$ which defines the shape of the aerofoil. Then it is evident from Fig.1 that the $X_0$ co-ordinate defining the position of B must satisfy the relation

$$X - X_0 = (Y - Y_0) \cot (\mu + \theta), \quad .. \quad .. \quad .. \quad .. \quad .. \quad .. \quad (19)$$

where $Y_0$, $\mu$, and $\theta$ are known functions of $X_0$. From (19) the appropriate value of $X_0$ for the point B associated with a particular point P($X$, $Y$) in the region of flow can be determined graphically or by an iterative method. For the biconvex circular-arc aerofoil considered, the following approximations are valid to the required order of accuracy

$$\left.\begin{aligned} Y_0 &= w(X_0 - X_0^2), \\ \theta &= w(1 - 2X_0). \end{aligned}\right\} \quad .. \quad .. \quad .. \quad .. \quad .. \quad .. \quad .. \quad (20)$$

It was also found that for high Mach numbers the following approximate formula could be used,

$$\cot \mu = \alpha + \beta X_0, \quad .. \quad .. \quad .. \quad .. \quad .. \quad .. \quad .. \quad (21)$$

where $\alpha$, $\beta$ are constants determined by the Mach number of the main flow upstream.

The coefficients $A_0$, $A_1$, . . . $B_0$, $B_1$, . . . of (14) vary from point to point in the field of flow, but the values appropriate to a particular point P are readily derived once the co-ordinate $X_0$ of the associated point B on the boundary is determined. Since $q_s$, $\theta$ are constant for all points on BP it follows immediately that along the characteristic line BP

$$\left.\begin{aligned} \frac{\partial q_s}{\partial R} &= -\cot (\mu + \theta + \Psi) \frac{1}{R} \frac{\partial q_s}{\partial \Psi}, \\ \frac{\partial \theta}{\partial R} &= -\cot (\mu + \theta + \Psi) \frac{1}{R} \frac{\partial \theta}{\partial \Psi}. \end{aligned}\right\} \quad .. \quad .. \quad .. \quad .. \quad .. \quad (22)$$

By the use of (14), (16), (18) and (22) the appropriate form of the differential equation (13) in the neighbourhood of any point B in the field of flow can be determined.

5. *Aerofoil at Incidence.*—It is interesting to note that (15) leads to a simple formula for the pressure distribution $p$ on an aerofoil at a small incidence $\alpha$ in terms of the local values of $p_s$, $\rho_s$, $q_s$, and $\mu_s$ along the surface of the aerofoil at zero incidence. Let $\phi$ represent the velocity potential of the small disturbance resulting from the change of incidence $\alpha$. Then, if $\partial/\partial s$, $\partial/\partial n$ refer to changes along and normal to the streamline through the point P in the field of flow, the velocity increments due to the disturbance will be

$$dq = \left[\left(q_s + \frac{\partial \phi}{\partial s}\right)^2 + \left(\frac{\partial \phi}{\partial n}\right)^2\right]^{1/2} - q_s = \frac{\partial \phi}{\partial s} \quad .. \quad .. \quad .. \quad .. \quad (23)$$

and $q\, d\theta = \partial \phi / \partial n$.

Substitution in (15) yields

$$\frac{\partial \phi}{\partial s} = -\frac{\partial \phi}{\partial n}\tan \mu_s , \qquad (24)$$

and since $\partial\phi/\partial n = -q_s\alpha$ on the surface of the aerofoil, it follows that the pressure difference $p - p_s$ due to incidence is given by

$$p - p_s = \rho_s q_s \frac{\partial \phi}{\partial s} = -\rho_s q_s^2 \tan \mu_s \,.\, \alpha . \qquad (25)$$

For small values of $\alpha$, (25) corresponds and is equivalent to Busemann's third-order formula for isentropic flow. To allow for the effect of the shock wave at the leading edge, the Busemann correction term (6) could be added to give

$$\frac{p - p_s}{\rho_0 q_0^2} = -\left[\left(\frac{\rho_s}{\rho_0}\right)\left(\frac{q_s}{q_0}\right)^2 \tan \mu + \tfrac{3}{2}Dw^2\right]\alpha , \qquad (26)$$

where

$w \equiv$ the semi-angle at the leading edge,

$$D \equiv \frac{(\gamma+1)M_0^4}{48(M_0^2-1)^{7/2}}\left[(5-3\gamma)M_0^4 + 4(\gamma-3)M_0^2 + 8\right], \qquad (27)$$

and $M_0$ is the Mach number of the main flow.

6. *Numerical Method of Solution.*—The method used to obtain the results given in this paper is based on the representation of (13) in difference form. The field of flow is divided by a system of lines drawn normal to the surface at equal intervals apart and by circular-arcs as shown below (Fig. 2).

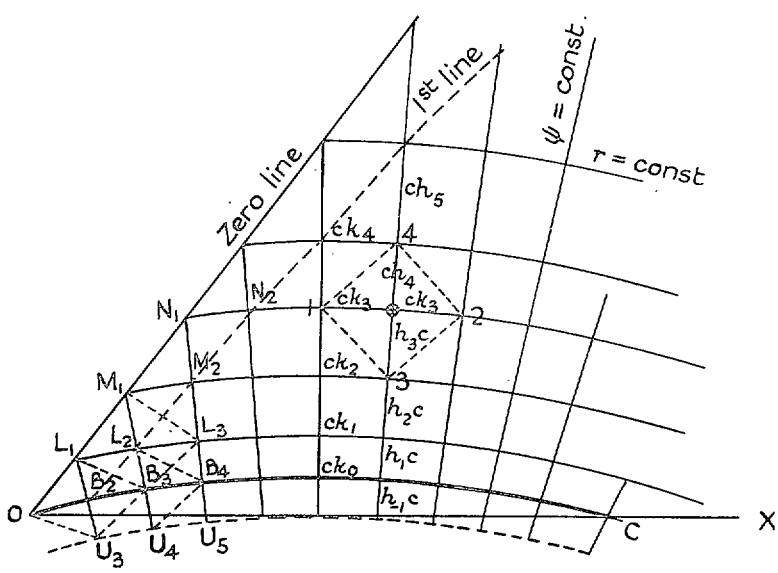


FIG. 2.

The normals to the aerofoil surface OBC intersect the leading Mach line OL at $L_1$, $M_1$, $N_1$, etc., and through these points circular-arcs are drawn—the circular-arcs all having a common centre O′ (*see* Fig. 1). Each circular-arc is divided into equal segments but the circular-arcs do not

cut the normals at equal intervals. For convenience the network is extended below the surface of the aerofoil to enable the boundary conditions to be represented numerically as differences. It can easily be shown that, in difference form,

$$\left.\begin{aligned} \frac{\partial \Phi}{\partial R} &= \left[\frac{\Phi(4)-\Phi(O)}{h^2_{n+1}} - \frac{\Phi(3)-\Phi(O)}{h_n^2}\right]\frac{h_n h_{n+1}}{h_n + h_{n+1}}, \\ \frac{1}{R}\frac{\partial \Phi}{\partial \Psi} &= \frac{\Phi(2)-\Phi(1)}{2k_n}, \end{aligned}\right\} \quad .. \quad .. \quad .. \quad (28)$$

$$\left.\begin{aligned} \frac{\partial^2 \Phi}{\partial R^2} &= \frac{2}{h_n h_{n+1}}\left[\frac{h_n \Phi(4) + h_{n+1}\Phi(3) - \Phi(O)(h_{n+1}+h_n)}{h_n + h_{n+1}}\right], \\ \frac{1}{R^2}\frac{\partial^2 \Phi}{\partial \Psi^2} &= \frac{\Phi(1)+\Phi(2)-2\Phi(O)}{k_n^2}, \end{aligned}\right\} \quad .. \quad .. \quad (29)$$

where $\Phi(1)$, $\Phi(2)$, $\Phi(3)$, $\Phi(4)$ denote the values of $\Phi$ at the corners of the typical cell marked in Fig. 2 and $\Phi(0)$ represents the value at the inside or 'centre' point O. The values of $h_n$, $k_n$ correspond to the cell under consideration and vary over the field of flow. By the use of (28) and (29), equation (13) can then be represented by a system of linear equations* relating the values of the $\Phi$'s over the whole field of flow.

Along OL, $\Phi = 0$, and it is assumed that in the neighbourhood of OL the solution approximates closely to that given by the flat plate theory for the Mach number $M_1$ of the deflected flow. On this basis the aerodynamic forces on a thin oscillating wedge in an airstream $M_0$ would correspond to the forces given by the flat plate theory for the Mach number $M_1$. This is certainly so in steady motion, for (25) is in effect Ackeret's formula with $\rho_0$, $q_0$, $\mu_0$ for the undisturbed main flow replaced by the local values $\rho_1$, $q_1$, $\mu_1$ for the wedge.

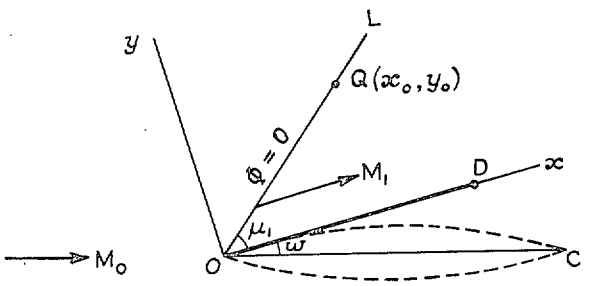


FIG. 3.

For a flat plate OD oscillating in an airstream of Mach number $M_1$, it can be shown that

$$\left.\begin{aligned} \frac{\partial}{\partial x}\Phi(Q) &= -\tan\mu_1 \frac{\partial \Phi(Q)}{\partial y} \\ &= -\tan\mu_1 \,.\, \exp\left(-i\lambda_1 \sec^2\mu_1 \, x_0\right) \,.\, \frac{\partial \Phi(O)}{\partial y} \end{aligned}\right\} \quad .. \quad .. \quad .. \quad (30)$$

where $\lambda_1 = pc/q_1$, $\operatorname{cosec}\mu_1 = M_1$, and where $\partial\Phi(O)/\partial y$ represents the boundary condition at $O$. At the origin,

$$\frac{\partial \Phi(O)}{\partial y} = \frac{\partial \Phi(O)}{\partial R}, \quad .. \quad .. \quad .. \quad .. \quad .. \quad .. \quad .. \quad .. \quad (31)$$

* The equations are used in complex form except when solutions for $\lambda_0 \to 0$ are required. Equation (13) is then replaced by two real equations for $M$ and $N$, where $\Phi = M + i\lambda_0 N$.

and the following general relations are valid

$$\left.\begin{aligned} \frac{1}{R}\frac{\partial\Phi(Q)}{\partial\Psi} &= -\tan(u+w+\Psi)\frac{\partial\Phi(Q)}{\partial R}, \\ \frac{\partial\Phi(Q)}{\partial R} &= \frac{\partial\Phi(Q)}{\partial y}\frac{\cos(u+w+\Psi)}{\cos\mu}, \\ \frac{\partial\Phi(Q)}{\partial y} &= \frac{\partial\Phi(O)}{\partial R}\cdot\exp(-i\lambda_1\sec^2\mu_1 x_0). \end{aligned}\right| \quad \ldots\ \ldots\ \ldots\ \ldots \quad (32)$$

By the use of (32) it is possible to estimate the derivatives of $\Phi$ at the points $L_1$, $M_1$, $N_1$, etc., on the leading Mach line since $\partial\Phi(O)/\partial R$ is known. When the centre points of the cells are on the line OL, at $N_1$ for instance, formulae (29) are replaced by

$$\left.\begin{aligned} \frac{\partial^2\Phi(N_1)}{\partial R^2} &= \frac{2}{h_3^2}\left[\Phi(M_2)+h_3\frac{\partial\Phi(N_1)}{\partial R}\right] \\ \frac{1}{R^2}\frac{\partial^2\Phi(N_1)}{\partial\Psi^2} &= \frac{2}{h_3^2}\left[\Phi(N_2)-h_3\frac{\partial\Phi(N_1)}{R\,\partial\Psi}\right], \end{aligned}\right| \quad \ldots\ \ldots\ \ldots\ \ldots \quad (33)$$

where $\partial\Phi(N_1)/\partial R$, $\partial\Phi(N_1)/\partial\Psi$ are given by (32) in terms of the boundary condition at $O$. Substitution of (33) in (13) leads to an equation for $\Phi(N_2)$ in terms of $\Phi(M_2)$ for the cell of centre $N_1$. Similarly, $\Phi(M_2)$ can be determined when $\Phi(L_2)$ is known, and $\Phi(L_2)$ when $\Phi(B_2)$ is determined. In the present calculations $\Phi(B_2)$ was assumed to have the value corresponding to that given by flat plate theory for the mean flow conditions over OB, and the values of $\Phi$ along $B_2N_2$ were then readily derived from the difference equations in the way already described. For the cell with centre at $B_2$, the finite difference form of (13) gives $\Phi(B_3)$ in terms of $\Phi(B_2)$ and $\Phi(U_3)$, where $\Phi(B_2)$ is assumed and

$$\Phi(U_3) = -2h_1\frac{\partial\Phi(B_2)}{\partial R}. \quad \ldots\ \ldots\ \ldots\ \ldots\ \ldots\ \ldots\ \ldots \quad (34)$$

Similarly, $\Phi(B_4)$ is given in terms of $\Phi(L_2)$, $\Phi(B_2)$, $\Phi(B_3)$ and $\Phi(U_4)$, where

$$\Phi(U_4) = \Phi(L_2) - 2h_1\frac{\partial\Phi(B_3)}{\partial R}. \quad \ldots\ \ldots\ \ldots\ \ldots\ \ldots\ \ldots\ \ldots \quad (35)$$

The value of $\partial\Phi/\partial R$ on the boundary is determined by the motion of the aerofoil.

With the aid of the preceding formula, it is possible to derive values of $\Phi$ along the aerofoil surface and hence to deduce the pressure distribution. The various stages of the calculation are listed below for reference :—

(1) Choice of spacing for the network.

(2) Determination of the $X$, $Y$ and $R$, $\Psi$ co-ordinates of the corners of the cells.

(3) Calculation of $q_s$, $\theta$ at each point of intersection of the normals and the circular-arcs.

(4) Calculation of $A_0$, $A_1$, $A_2$, $A_3$ and $B_0$, $B_1$, $B_2$ for each point by the use of (14).

(5) Estimation of $\Phi(B_2)$ as suggested and the calculation of the first derivatives of $\Phi$ along OL by (30).

(6) Determination of $\Phi(L_2)$, $\Phi(M_2)$, etc., along the first line by use of the above results and a particular difference form of (13).

(7) Calculation of $\Phi$ values over the network using the full form of the difference equations and the appropriate surface boundary conditions.

(8) Determination of the pressure distribution.

(9) Calculation of the aerodynamic derivative coefficients.

7. *Boundary Conditions.*—Let us suppose the aerofoil is describing translational and pitching oscillations

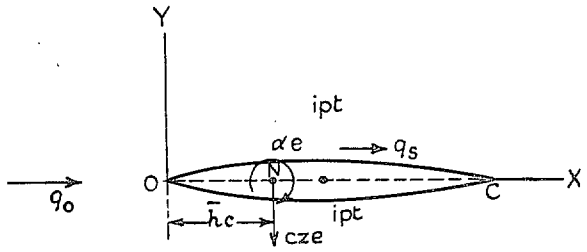


FIG. 4.

as shown in Fig. 4, where the point N distant $\bar{h}c$ from the leading edge denotes the position of the axis of oscillation. The velocity distribution $q_s$ corresponding to steady flow at zero incidence is known, and the condition for tangential flow at the upper surface when the aerofoil is oscillating can be expressed as

$$-\frac{\partial \Phi}{c\,\partial R} = q_s\alpha + iq_0\lambda_0(X - \bar{h})\,\alpha + iq_0\lambda_0 z \qquad (36)$$

when terms of order $\alpha\Psi^2$, $z\Psi^2$ are neglected. The amplitudes of oscillation are assumed to be small and, since the aerofoil in the case considered is only 5 per cent thick, (36) can be regarded as being correct to second order. To this order of accuracy, the shape of the aerofoil section only affects the first term in (36). For convenience, let the velocity potential $\Phi$ for the flow above the wing be represented in the form

$$\Phi = -c[\alpha q_1\Phi_1 + iq_0\lambda_0\alpha\Phi_2 + iq_0\lambda_0(z - \bar{h}\alpha)\,\Phi_3]\,. \qquad (37)$$

The symbols $\Phi_1$, $\Phi_2$, $\Phi_3$ respectively are the velocity potentials corresponding to the boundary conditions

$$\frac{\partial \Phi_1}{\partial R} = \frac{q_s}{q_1}, \qquad (38)$$

$$\frac{\partial \Phi_2}{\partial R} = X\,, \qquad (39)$$

$$\frac{\partial \Phi_3}{\partial R} = 1\,, \qquad (40)$$

where $q_1$ in (38) represents the speed of the deflected airstream at the leading edge when the aerofoil is fixed at zero incidence. When the solutions of (13) corresponding to (38), (39), (40) have been determined, the general solution corresponding to simple harmonic motion of the aerofoil is given by (37).

For the case of an aerofoil at incidence in steady flow the right-hand side of equation (13) vanishes and the general solution of the reduced equation for boundary condition (38) above should agree with the known exact solution for isentropic conditions.

8. *Aerodynamic Derivatives.*—The pressure distribution over the aerofoil's surface can be derived from equation (6) as follows: Let $p_s$, $\rho_s$, $q_s$ represent the local pressure, density and velocity at the aerofoil's surface when at zero incidence. Then, if $\phi$ represents the potential of a small disturbance, it can be deduced from (6) that the pressure change $p - p_s$ at a particular point is given by

$$p - p_s = -\rho_s\left(\frac{\partial \phi}{\partial t} + q_s\frac{\partial \phi}{\partial s}\right), \qquad (41)$$

where $\partial\phi/\partial s$ defines the rate of change of $\phi$ along the surface of the aerofoil. From (41) it follows that the lift distribution

$$l(x) = p - p_u = 2\rho_s\left(\frac{\partial \phi_u}{\partial t} + q_s\frac{\partial \phi_u}{\partial s}\right), \qquad (42)$$

where the suffix $u$ refers to the upper surface and $l$ to the lower. Then, to second-order accuracy in the displacements and the thickness/chord ratio (R. & M. 2679[6]), it can be shown that the total lift $L$ and pitching moment $M$ about the reference point are given by

$$\left.\begin{aligned} L &= c\int_0^1 (p_l - p_u)\,dX \\ M &= -c^2\int_0^1 (p_l - p_u)(X-h)\,dX. \end{aligned}\right\} \quad .. \quad .. \quad .. \quad (43)$$

Since $\phi = \Phi e^{ipt}$ and $\lambda_0 = pc/q_0$, (42) can be expressed in the form

$$\frac{l(X)}{\rho_0 q_0} = \frac{2}{c}\left(\frac{\rho_s}{\rho_0}\right)\left[i\lambda_0\phi + \left(\frac{q_s}{q_0}\right)\frac{\partial\phi}{\partial X}\right], \quad .. \quad .. \quad .. \quad .. \quad .. \quad (44)$$

when $s = cX$ is substituted. By the use of (37) and (44), equations (43) lead to expressions for the amplitudes $L'$, $M'$ of the lift and pitching moment of the form

$$\frac{L'}{\rho_0 c q_0^2} = -2\int_0^1 \left(\frac{\rho_s}{\rho_0}\right)\left\{\alpha\left[\frac{q_1}{q_0}.L_1 + i\lambda_0(L_2 - \bar{h}L_3)\right] + i\lambda_0 z L_3\right\}dx \quad .. \quad (45)$$

$$\frac{M'}{\rho_0 c^2 q_0^2} = 2\int_0^1 \left(\frac{\rho_s}{\rho_0}\right)\left\{\alpha\left[\frac{q_1}{q_0}.L_1 + i\lambda_0(L_2 - \bar{h}L_3)\right] + i\lambda_0 L_3 z\right\}(X-\bar{h})\,dX, \quad .. \quad .. \quad (46)$$

where $L_1 = i\lambda_0\Phi_1 + \frac{q_s}{q_0}\cdot\frac{\partial\Phi_1}{\partial X}$, etc. From (45) and (46), the values of the derivatives can be determined. In the notation of R. & M. 2140[3] and 2679[6]

$$\frac{L'}{\rho_0 c q_0^2} = (l_z + i\lambda_0 l_{\dot{z}})z + (l_\alpha + i\lambda_0 l_{\dot{\alpha}})\alpha \quad .. \quad .. \quad .. \quad .. \quad .. \quad (47)$$

$$\frac{M'}{\rho_0 c^2 q_0^2} = (m_z + i\lambda_0 m_{\dot{z}})z + (m_\alpha + i\lambda_0 m_{\dot{\alpha}})\alpha \quad .. \quad .. \quad .. \quad .. \quad (48)$$

so that when the complex coefficients of $z$ and $\alpha$ in (45) and (46) have been calculated the values of the derivative coefficients $l_z$, $l_{\dot{z}}$, $m_\alpha$, $m_{\dot{\alpha}}$, $m_z$, $m_{\dot{z}}$, $l_\alpha$, $l_{\dot{\alpha}}$ can readily be derived.

9. *Numerical Applications.*—The method of solution suggested was used to calculate the pressure distribution and the lift and pitching-moment derivatives for a biconvex, symmetrical, circular-arc aerofoil of 5 per cent thickness/chord ratio. In order to test the reliability of the method, network solutions were first obtained for the following cases—

(*a*) an oscillating flat plate*,

(*b*) an aerofoil at incidence in steady flow,

and they are compared with the known exact solutions in Figs. 5 and 6. It was found that the network obtained by dividing the surface of the aerofoil into ten equal segments was sufficiently fine. The results show good agreement with the exact solutions for (*a*) and (*b*), and in view of this it is believed that the solutions obtained for the oscillating thick aerofoil are reasonably accurate. As the speed decreases, however, the leading Mach line OL increases in slope and the network becomes rather extended in the direction normal to the surface. For the lower values of $M_0$ a finer network might have to be used.

In the determination of the pressure distribution from the calculated values of $\Phi$, it was found advisable to represent $\Phi$ as a quartic in $X$ of the form

$$\Phi = \alpha X + \beta X^2 + \gamma X^3 + \delta X^4, \quad .. \quad .. \quad .. \quad (49)$$

where $\alpha\,[\equiv (\partial\Phi/\partial X)_{X=0}]$ was chosen to give the correct value at the leading edge. The best values of $\beta$, $\gamma$, $\delta$ were then determined by the least-squares method. In all cases it was found that the

* In both cases the values of $\partial\phi/\partial x$ and $\partial\phi/\partial y$ along OL and of $\phi_B$ were assumed as suggested in section 6.

values given by (49) agreed well with those derived from the network. Since slight irregularities in $\Phi$ lead to marked irregularities in $\partial\Phi/\partial X$ when differences are taken, the values of $\partial\Phi/\partial X$ were deduced from (49) rather than by differencing.

For the particular aerofoil considered the theory breaks down at about $M = 1{\cdot}3$ as the flow at the leading edge is then subsonic. However, it is thought that the values for the aerodynamic derivatives given in this report for $M_0 = 1{\cdot}4$, $1{\cdot}5$ and $2{\cdot}0$ are reliable within the limitations of inviscid, isentropic, irrotational flow theory. Values of $-m_a$ and $-m_{\dot{a}}$ are plotted in Figs. 8, 9 and 10 for various values of $\lambda_0$, and it will be noted that the values of the damping coefficient $-m_{\dot{a}}$ are larger at the lower Mach numbers, but slightly lower at the highest Mach number, than those given by the flat plate theory. The variation in $-m_{\dot{a}}$ with the position of the axis of oscillation is shown in Figs. 11a, b and c, for certain values of $M_0$ and $\lambda_0$. Similar curves for the other derivative coefficients are given in Figs. 12 to 14.

10. *Concluding Remarks.*—The results show that thickness has a marked effect on the aerodynamic derivatives for a two-dimensional aerofoil and, in view of this, some allowance for such an effect should be made in flutter and stability calculations. For oscillations about the half-chord axis, the value of the damping coefficient $-m_{\dot{a}}$ is increased, but for more forward axis positions, thickness appears to have the opposite effect. According to the flat plate theory the damping is positive for oscillations about the leading edge, when $M \geqslant \sqrt{2}$ but Fig. 11b shows that the damping for the thick aerofoil is still negative at $M = 1{\cdot}5$. This indicates that the range of Mach number and axis position for which it is possible to get one degree of freedom instability would be dependent on the thickness of the aerofoil.

In R. & M. 2679[6] it was assumed that the effect of thickness was independent of the frequency parameter. This is approximately true as far as the pitching-moment aerodynamic-stiffness coefficient is concerned, but the results for $-m_{\dot{a}}$ shown in Fig. 9c, for instance, give an initial decrease in the amount of correction due to thickness followed by an increase as the frequency parameter $\lambda_0$ increases.

Measurements of aerodynamic damping on oscillating aerofoils in two dimensions and on half-delta wings are to be made at the National Physical Laboratory. These tests will provide a control on present theory and a guide to further development. An attempt to allow for thickness effects on derivatives for a wing of finite aspect ratio could be made by the use of strip theory in conjunction with the present method. Such a procedure may, however, not be valid in general and one must look to experiment for guidance on this question, particularly in the case of low aspect ratio wings.

## REFERENCES


| *No.* | *Author* | *Title, etc.* |
|---|---|---|
| 1 | J. B. Bratt and A. Chinneck .. .. | Information Report on Measurements of Mid-chord Pitching Moment Derivative at High Speeds. July, 1947. A.R.C. Report 10,710. (Unpublished.) |
| 2 | W. A. Mair and J. A. Beavan .. .. | *Modern Developments in Fluid Dynamics.* Vol. III, Chapter XII. Flow Past Aerofoils and Cylinders. August, 1948. A.R.C. Report 11,692. (Unpublished.) |
| 3 | G. Temple and H. A. Jahn .. .. | Flutter at Supersonic Speeds. Part I. Mid-chord Derivative Coefficients for a Thin Aerofoil at Zero Incidence. R. & M. 2140. April, 1945. |
| 4 | W. P. Jones .. .. .. .. | Supersonic Theory for Oscillating Wings of Any Plan Form. R. & M. 2655. June, 1948. |
| 5 | Edmonson, Murnaghan and Snow .. | The Theory and Practice of Two-dimensional Supersonic Pressure Calculations. John Hopkins University Applied Physics Laboratory. Bumblebee Report No. 26. |
| 6 | W. Prichard Jones .. .. .. | The Influence of Thickness/Chord Ratio on Supersonic Derivatives for Oscillating Aerofoils. R. & M 2679. September, 1947. |

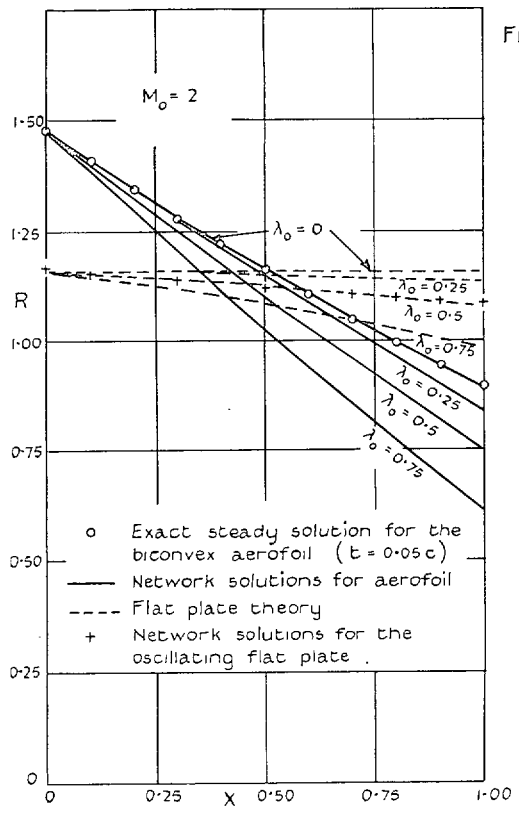


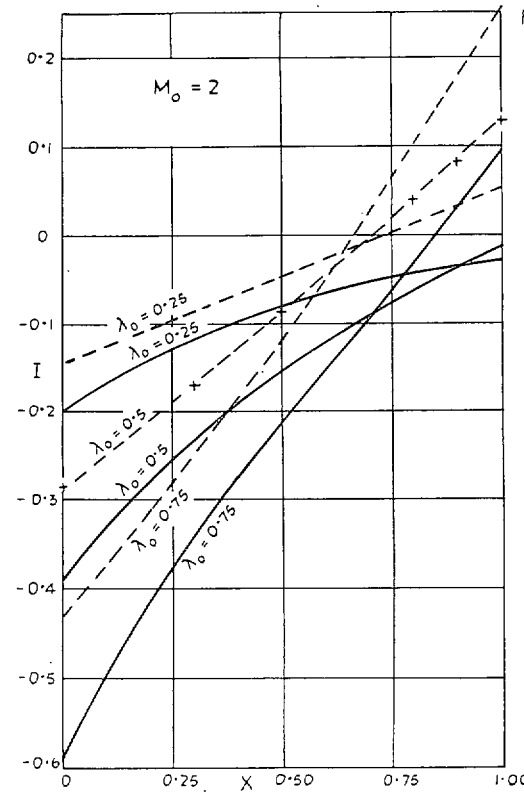


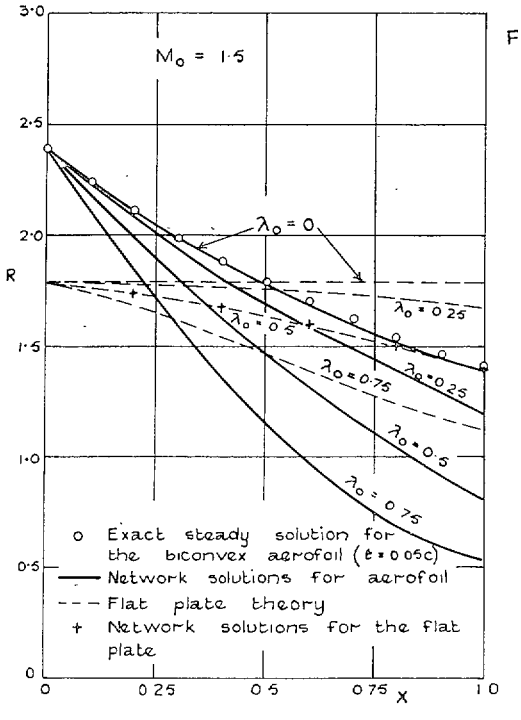


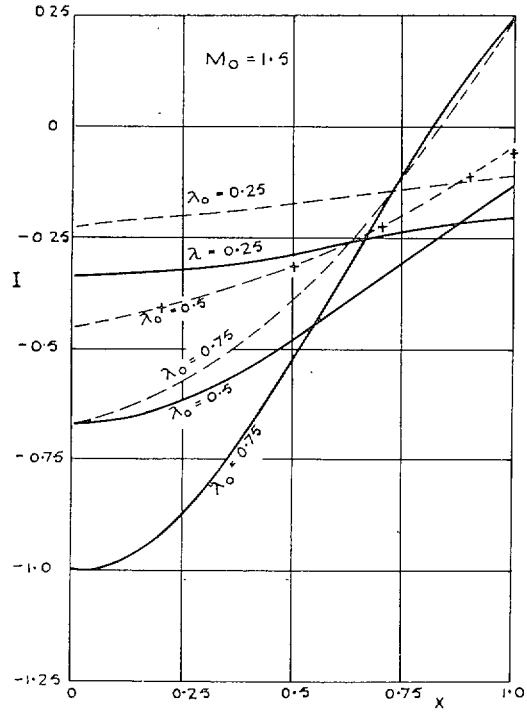


FIGS. 5a, 5b, 6a and 6b. Values of $\frac{l(X)}{\alpha \rho_0 q_0^2}$ ($\equiv R + iI$) for oscillations about the mid-chord axis.

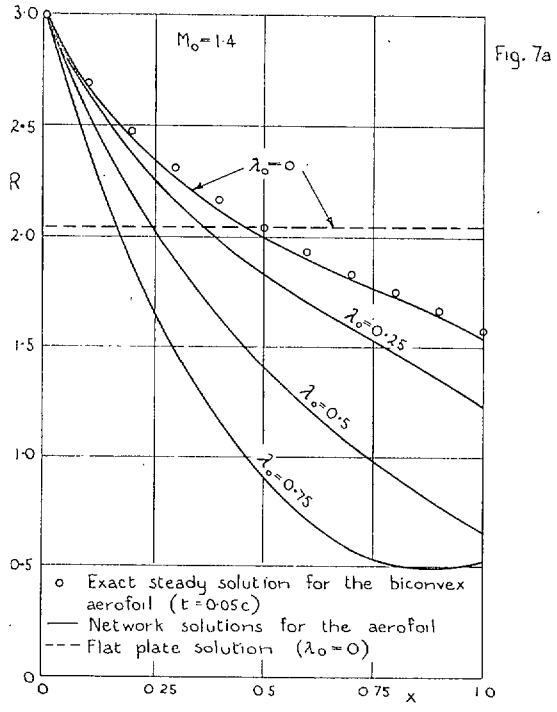


Fig. 7a

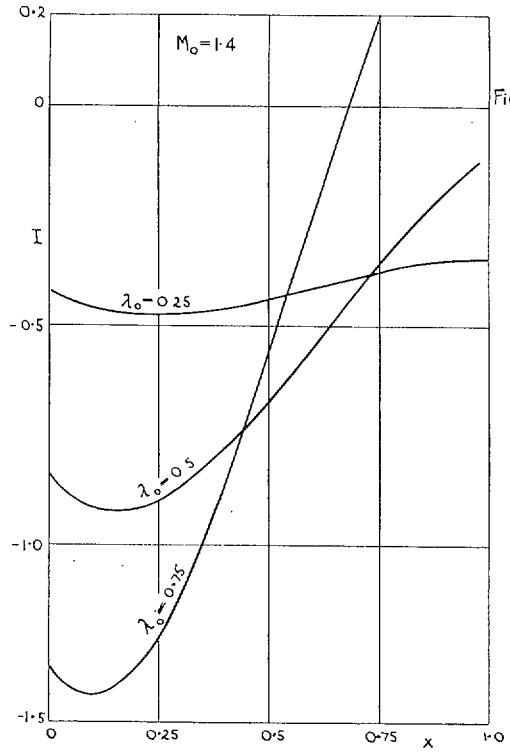


Fig. 7b

FIGS. 7a and 7b. Values of $\frac{l(X)}{\alpha \rho_0 q_0^2}$ ($\equiv R + iI$) for oscillations about the mid-chord axis.

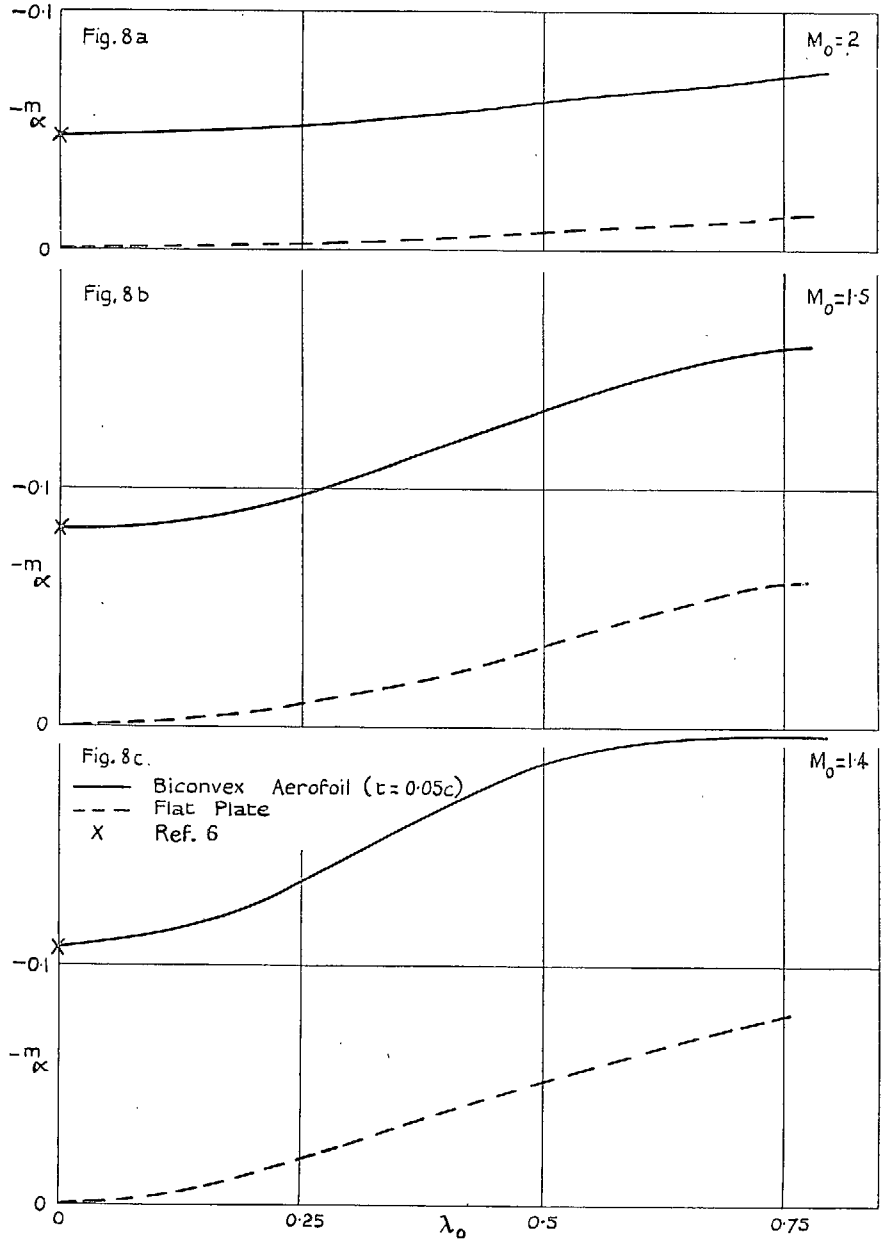


FIGS. 8a, 8b and 8c. Values of the aerodynamic stiffness coefficient for pitching oscillations about the mid-chord axis.

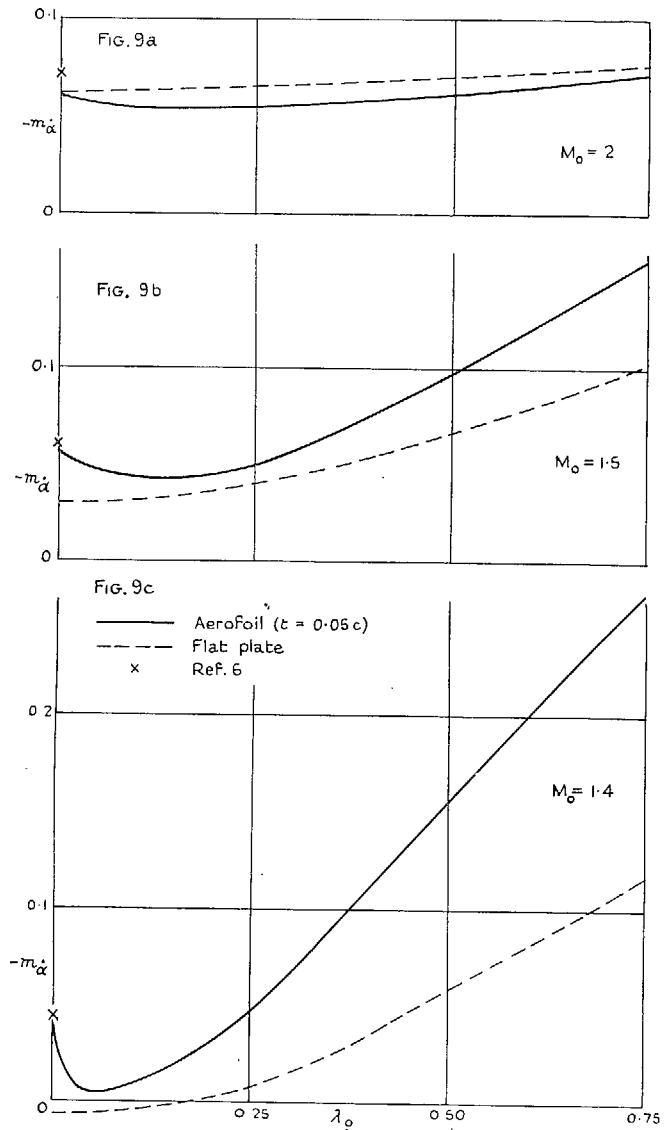


FIGS. 9a, 9b and 9c. Values of the aerodynamic damping coefficient for pitching oscillations about the mid-chord axis.

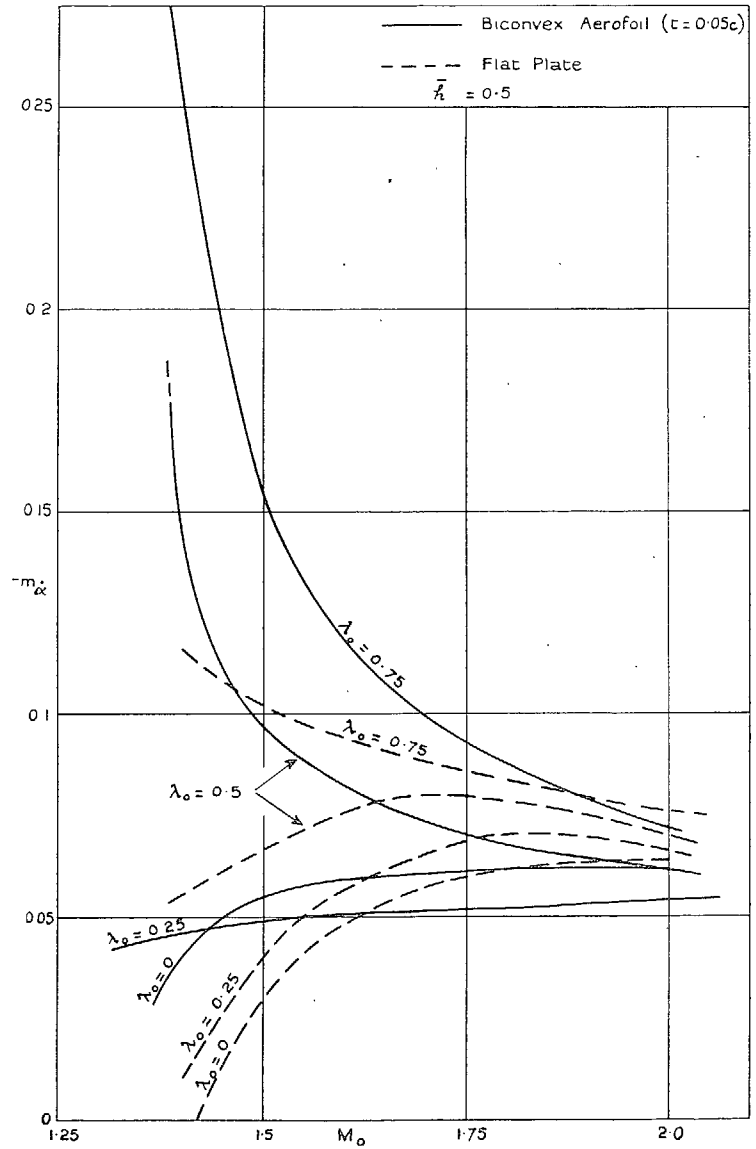


FIG. 10. Variation in the coefficient $-m_{\dot{\alpha}}$ with Mach number.

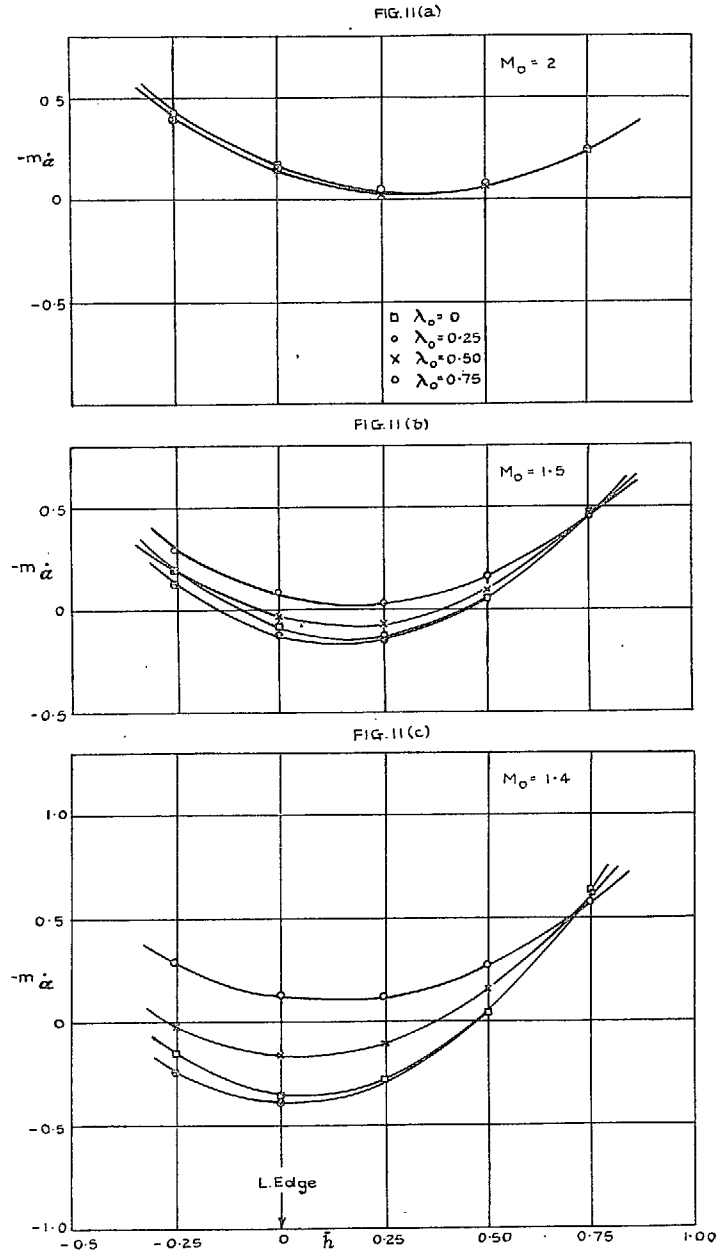


FIGS. 11a, 11b and 11c. Variation in the coefficient $-m_{\dot{\alpha}}$ with axis position.

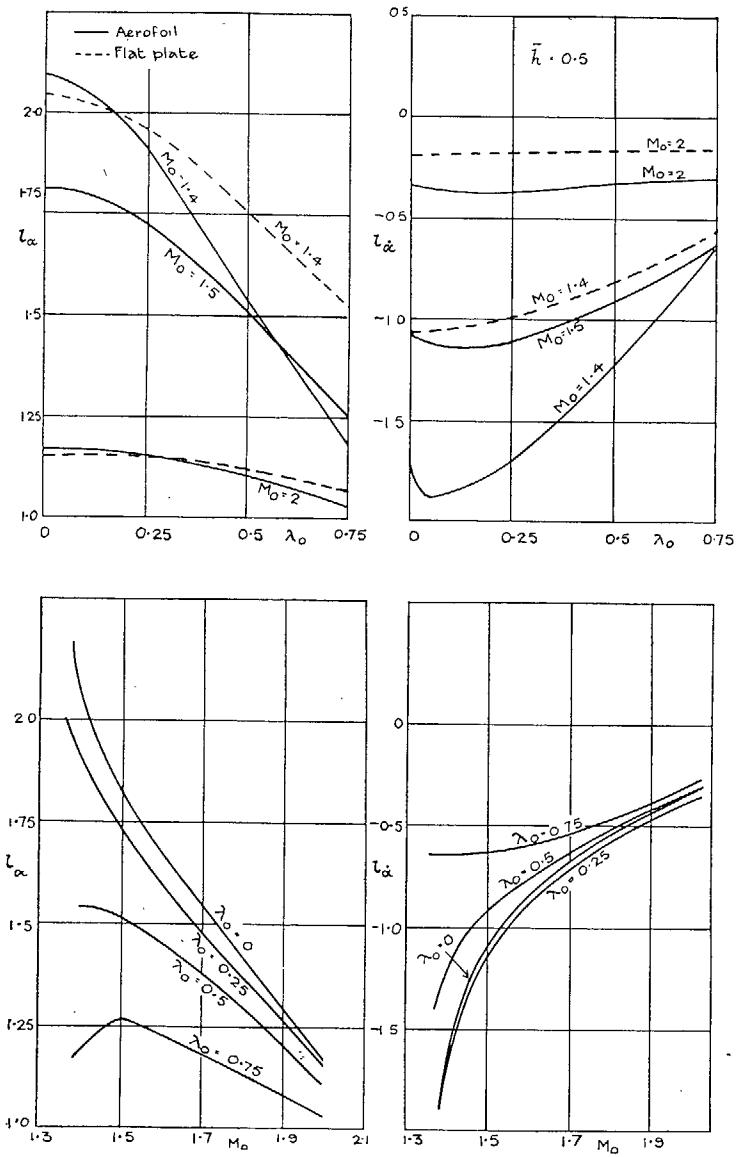


FIG. 12. Values of the coefficients $l_a$ and $l_{\dot a}$.

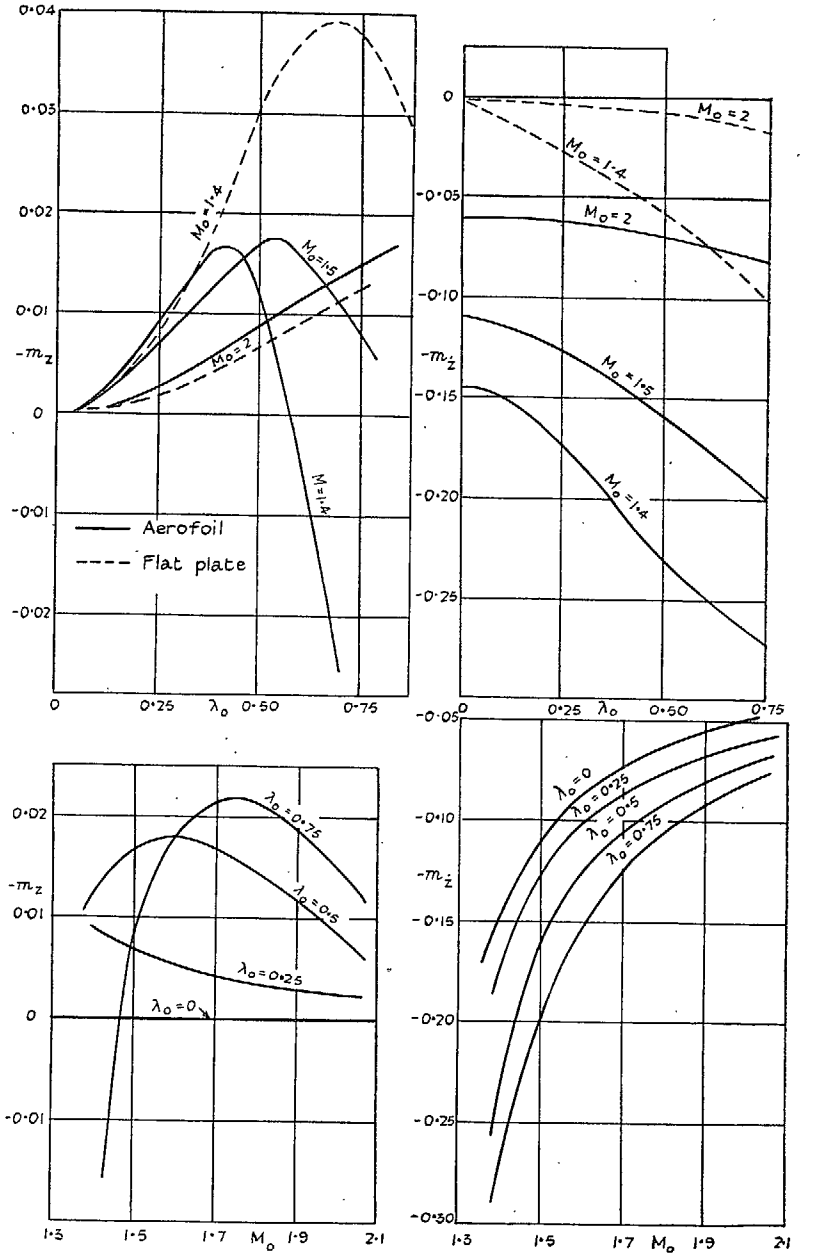


FIG. 13. Values of the coefficients $-m_z$ and $-m_{\dot z}$.

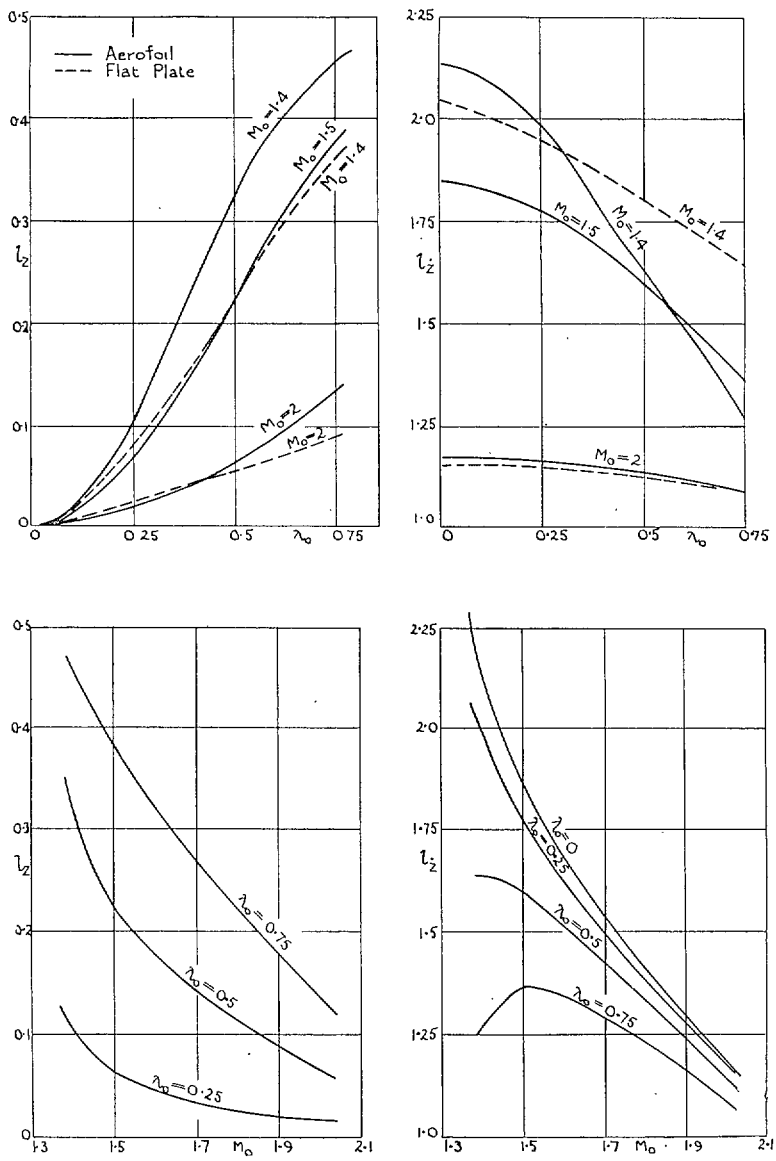


FIG. 14. Values of the coefficients $l_z$ and $l_{\dot{z}}$.

# The Effect of Thickness on the Aerodynamic Forces on Biconvex Aerofoils Oscillating in a Supersonic Airstream, and Calculation of Forces for Aerofoil with Flap*

*By*

SYLVIA W. SKAN,

of the Aerodynamics Division, N.P.L.

*Summary.*—The lift distribution and the aerodynamic force coefficients are calculated for a 7·5 per cent thick symmetrical circular-arc aerofoil at Mach numbers $M_0 = 2{\cdot}0,\ 1{\cdot}7,\ 1{\cdot}5$ for a range of frequencies. These results are compared with those given in an earlier report (Ref. 1) for a 5 per cent thick aerofoil, and with the values derived on the basis of flat plate theory.

A limited comparison is also made between the calculated results and those obtained experimentally.

The same scheme of computation is then applied to the determination of the derivatives for an aerofoil with a flap hinged at 0·6 chord from the aerofoil leading edge, for $M_0 = 1{\cdot}7$ only. The values thus obtained for the 7·5 per cent and the 5 per cent thick aerofoils are compared with the limiting values for $\lambda_0$ tending to 0 derived by Temple and Jahn for a thin aerofoil with flap (Ref. 2), and with the two-dimensional derivatives calculated for several values of $\lambda_0$ from formulae given in a paper by Huckel and Durling (Ref. 5).

1. *Introduction.*—Isentropic, irrotational and inviscid flow conditions are assumed. The known flow at zero incidence is slightly disturbed, and the non-linear equation defining the resulting motion is reduced to linear form. The differential equation thus obtained is put into difference form, and is solved by a step-by-step process to give $\Phi$, the amplitude of the velocity potential of the disturbance. For the numerical applications given here and in Ref. 1, the field of flow is divided into a network by lines drawn normal to the surface of the aerofoil through ten equally spaced points and by circular-arcs parallel to the surface.

The derivation of the differential equation and the numerical method of solution are described in detail in Ref. 1. The same notation is used here as in Ref. 1, and a list of symbols is given below.

*List of Symbols*

| | |
|---|---|
| $M_0$ | Mach number |
| $q_0$ | Velocity of undisturbed main flow |
| $\rho_0$ | Air density in undisturbed main flow |
| $c$ | Chord of aerofoil |
| $t$ | Thickness of biconvex aerofoil at mid-chord |
| $r = cR$ | Radius of a circular-arc of the network |
| $w$ | Semi-wedge angle |
| $q_1$ | Velocity of deflected airstream at leading edge when aerofoil is at zero incidence |
| $q_s$ | Local undisturbed velocity |
| $\rho_s$ | Local air density |

*Published with the permission of the Director, National Physical Laboratory.
A.R.C. Report No. 14,217. August, 1951.

*List of Symbols*—continued

| | |
|---|---|
| $\mu_s$ | Local Mach angle |
| $p/2\pi$ | Frequency in cycles per second |
| $\lambda_0 \left(\equiv \frac{pc}{q_0}\right)$ | Frequency parameter |
| $\phi\ (\equiv \Phi e^{ipt})$ | Velocity potential of disturbance |
| $cX$ | Distance measured along aerofoil from leading edge |
| $c\bar{h}$ | Distance of axis of oscillation of aerofoil from its leading edge |
| $cze^{ipt}$ | Vertical displacement of aerofoil |
| $\alpha e^{ipt}$ | Angular displacement of aerofoil as a whole |
| $cX_f$ | Distance of a point P on the flap from the hinge |
| $c\bar{H}$ | Distance of flap hinge from leading edge of aerofoil |
| $\beta e^{ipt}$ | Angular displacement of flap relative to aerofoil |
| $l(X)\ [\equiv \alpha\rho_0 q_0^2\ (R + iI)]$ | Lift distribution |
| $L\ (\equiv L'e^{ipt})$ | Total lift |
| $M\ (\equiv M'e^{ipt})$ | Pitching moment |
| $H\ (\equiv H'e^{ipt})$ | Flap hinge moment |

2. *Estimation of Accuracy.*—The method developed in Ref. 1 was used there to determine the forces on a 5 per cent thick aerofoil for Mach numbers $M_0 = 2{\cdot}0$, $1{\cdot}5$, $1{\cdot}4$, and additional values are given here for $M_0 = 1{\cdot}7$ and $\lambda_0 = 0$. For this aerofoil, which has a wedge angle of about $11{\cdot}4$ deg, the flow at the leading edge becomes subsonic, and the theory thus breaks down, at about $M_0 = 1{\cdot}3$. For the higher thickness/chord ratio of $7{\cdot}5$ per cent, corresponding to a wedge angle of about $17{\cdot}2$ deg, the flow at the leading edge is subsonic when $M_0$ is just under $1{\cdot}4$, and the calculations for this aerofoil cannot be carried much below $M_0 = 1{\cdot}5$.

In order to gain some idea of the degree of accuracy to be expected, the estimated lift distribution for steady motion is plotted in Fig. 1 for the 5 per cent and the $7{\cdot}5$ per cent thick aerofoils, together with the known exact solutions. At $M_0 = 2{\cdot}0$, $1{\cdot}7$, and $1{\cdot}5$ for the thinner aerofoil, and $M_0 = 2{\cdot}0$ and $1{\cdot}7$ for the thicker aerofoil, agreement between the estimated and the exact values is extremely good. For the thicker aerofoil at $M_0 = 1{\cdot}5$ the maximum error over the range $X = 0$ to $X = 0{\cdot}9$ is about 5 per cent (at $X = 0{\cdot}4$), compared with about $2{\cdot}6$ per cent (at $X = 0{\cdot}4$) for the thinner aerofoil at $M_0 = 1{\cdot}4$. The slightly greater divergence of the estimated curves at $X = 1$ is due to the fact that the $\Phi$ values obtained from the network were represented as a quartic to facilitate the determination of $\partial\Phi/\partial X$.

It is probable that better agreement would be obtained at the lower values of $M_0$ if a finer network were employed.

3. *Discussion of Results for Rigid Aerofoils.*—Values of the mid-chord derivatives for the 5 per cent thick aerofoil (Ref. 1) are given in Table 1, and the values obtained here for the $7{\cdot}5$ per cent thick aerofoil are given in Table 2. Comparisons between the results for the two aerofoils and those for the flat plate are represented graphically in Figs. 2–12.

Figs. 2 and 3 give the chordwise lift distribution for $M_0 = 2{\cdot}0$ and $M_0 = 1{\cdot}5$. Numerical results were obtained for $\lambda_0 = 0$, $0{\cdot}25$, $0{\cdot}5$, $0{\cdot}75$; but, in order not to confuse the diagrams,

only extreme values of $\lambda_0$ are included. The diagrams show that the thickness effect on the lift distributions $R$ and $I$ is reasonably linear when $M_0 = 2{\cdot}0$, but that there is a more rapid variation with thickness when $M_0 = 1{\cdot}5$.

In Figs. 4 and 5 the aerodynamic stiffness coefficient $-m_\alpha$ and the damping coefficient $-m_{\dot\alpha}$ for pitching oscillations about the mid-chord axis are plotted against $\lambda_0$ for $M_0 = 2{\cdot}0$ and $M_0 = 1{\cdot}5$.

It will be seen from Fig. 4 that the variation of the coefficient $-m_\alpha$ with thickness is approximately linear for both values of $M_0$. Fig. 5 shows, however, that the variation of $-m_{\dot\alpha}$ with thickness deviates considerably from a linear law, especially at the higher frequencies and lower Mach number. This effect is shown more clearly in Fig. 6, where $-m_{\dot\alpha}$ is plotted against the thickness/chord ratio for constant $\lambda_0$. It will be noted also from Fig. 6 that the value of $-m_{\dot\alpha}$ for the mid-chord axis position falls slightly as the thickness increases at $M_0 = 2{\cdot}0$, but that there is a definite increase of $-m_{\dot\alpha}$ with thickness at $M_0 = 1{\cdot}5$.

Fig. 7 shows the variation of $-m_{\dot\alpha}$ with $M_0$ for various values of $\lambda_0$, together with the flat plate results for $\lambda_0 = 0$, and experimental results for $\lambda_0$ tending to 0 taken from Ref. 3. It will be seen from Fig. 8, where $-m_{\dot\alpha}$ is plotted against $\bar h$ for $M_0 = 1{\cdot}5$ and $\lambda_0$ tending to 0, that the mid-chord axis position is relatively sensitive and that a small change of axis position would give close agreement between theory and experiment. Fig. 7 may thus give a misleading impression of the divergence between the present theory and the available experimental results.

In Fig. 9, $-m_\alpha$ is plotted against $\bar h$ for $M_0 = 1{\cdot}5$ and $\lambda_0$ tending to 0, and the results again show that a small change of axis position would give good agreement between theory and experiment. It will be seen that Hilton's static measurement is nearer to the theoretical value than Bratt's oscillatory measurement.

The other derivative coefficients are plotted against $\lambda_0$ for constant $M_0$, and against $M_0$ for constant $\lambda_0$, in Figs. 10–12.

4. *Force and Moment Derivatives for Aerofoil with Flap.*—

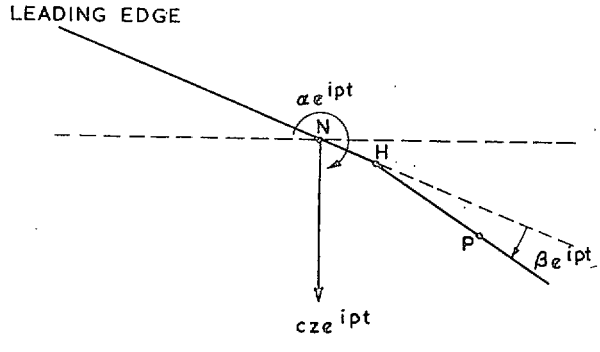


The diagram above shows the motions of an aerofoil carrying a flap. The aerofoil as a whole is describing translational and pitching oscillations about an axis N at a distance $c\bar h$ from the leading edge of the aerofoil. In addition, the flap is oscillating about its hinge H, distant $c\bar H$ from the leading edge of the aerofoil. $X_f$ denotes the distance of a point P on the flap from the hinge. The angles $\alpha$ and $\beta$ are assumed to be small and are exaggerated in the diagram.

The condition for tangential flow at the upper surface, corresponding to equation (36) of Ref. 1, is now

$$-\frac{1}{c}\frac{\partial \Phi}{\partial \bar R} = q_s\alpha + iq_0\lambda_0(X - \bar h)\alpha + iq_0\lambda_0 z \text{ when } X < \bar H$$

$$= q_s\alpha + iq_0\lambda_0(X - \bar h)\alpha + iq_0\lambda_0 z + q_s\beta + iq_0\lambda_0 X_f\beta \text{ when } X \geqslant \bar H\,. \qquad (1)$$

The velocity potential $\Phi_0$ for flow above the aerofoil as a whole, and the additional velocity potential $\Phi_f$ for the flap, are represented in the form

$$\Phi_0 = -c\,[\alpha q_1 \Phi_1 + iq_0\lambda_0\alpha\Phi_2 + iq_0\lambda_0(z - \bar{h}\alpha)\Phi_3] \quad .. \quad .. \quad .. \quad (2a)$$

$$\Phi_f = -c\,[\beta q_1 \Phi_{1\beta} + iq_0\lambda_0\beta\Phi_{2\beta}]$$

$$= 0 \text{ when } X \leqslant \bar{H}\,, \quad .. \quad .. \quad .. \quad .. \quad .. \quad .. \quad .. \quad (2b)$$

where $\Phi_1$, $\Phi_2$, $\Phi_3$ correspond to the boundary conditions

$$\frac{\partial\Phi_1}{\partial R} = \frac{q_s}{q_1},$$

$$\frac{\partial\Phi_2}{\partial R} = X\,,$$

$$\frac{\partial\Phi_3}{\partial R} = 1\,;$$

and the boundary conditions over the flap corresponding to $\Phi_{1\beta}$ and $\Phi_{2\beta}$ are

$$\left.\begin{aligned}\frac{\partial\Phi_{1\beta}}{\partial R} &= \frac{q_s}{q_1},\\ \frac{\partial\Phi_{2\beta}}{\partial R} &= X_f\,.\end{aligned}\right\} \quad .. \quad .. \quad .. \quad .. \quad .. \quad .. \quad .. \quad .. \quad (3)$$

The lift distribution is given by

$$\frac{l(X)}{\rho_0 q_0} = \frac{2}{c}\frac{\rho_s}{\rho_0}\left[i\lambda_0\phi + \frac{q_s}{q_0}\frac{\partial\phi}{\partial X}\right], \quad .. \quad .. \quad .. \quad .. \quad .. \quad .. \quad (4)$$

where $\phi$ represents the potential of a small disturbance.

Equations (2) and (4) lead to the following expressions for the amplitudes of the lift and moments

$$\frac{L'}{\rho_0 c q_0^2} = -2\int_0^1 \frac{\rho_s}{\rho_0}\left\{\alpha\left[\frac{q_1}{q_0}L_1 + i\lambda_0\,(L_2 - \bar{h}L_3)\right] + i\lambda_0 z L_3\right\} dX$$

$$- 2\int_{\bar{H}}^1 \frac{\rho_s}{\rho_0}\left\{\beta\left[\frac{q_1}{q_0}L_{1\beta} + i\lambda_0 L_{2\beta}\right]\right\} dX$$

$$\equiv (l_z + i\lambda_0 l_{\dot{z}})z + (l_\alpha + i\lambda_0 l_{\dot{\alpha}})\alpha + (l_\beta + i\lambda_0 l_\beta)\beta\,, \quad .. \quad .. \quad .. \quad (5)$$

$$\frac{M'}{\rho_0 c^2 q_0^2} = 2\int_0^1 \frac{\rho_s}{\rho_0}\left\{\alpha\left[\frac{q_1}{q_0}L_1 + i\lambda_0(L_2 - \bar{h}L_3)\right] + i\lambda_0 z L_3\right\}(X - \bar{h})\,dX$$

$$+ 2\int_{\bar{H}}^1 \frac{\rho_s}{\rho_0}\left\{\beta\left[\frac{q_1}{q_0}L_{1\beta} + i\lambda_0 L_{2\beta}\right]\right\}(X - \bar{h})\,dX$$

$$\equiv (m_z + i\lambda_0 m_{\dot{z}})z + (m_\alpha + i\lambda_0 m_{\dot{\alpha}})\alpha + (m_\beta + i\lambda_0 m_\beta)\beta\,, \quad .. \quad .. \quad (6)$$

$$\frac{H'}{\rho_0 c^2 q_0^2} = 2\int_{\bar{H}}^1 \frac{\rho_s}{\rho_0}\left\{\alpha\left[\frac{q_1}{q_0}L_1 + i\lambda_0(L_2 - \bar{h}L_3)\right] + i\lambda_0 z L_3\right\} X_f\,dX$$

$$+ 2\int_{\bar{H}}^1 \frac{\rho_s}{\rho_0}\left\{\beta\left[\frac{q_1}{q_0}L_{1\beta} + i\lambda_0 L_{2\beta}\right]\right\} X_f\,dX$$

$$\equiv (h_z + i\lambda_0 h_{\dot{z}})z + (h_\alpha + i\lambda_0 h_{\dot{\alpha}})\alpha + (h_\beta + i\lambda_0 h_\beta)\beta\,, \quad .. \quad .. \quad (7)$$

where $L_1 = i\lambda_0\Phi_1 + \frac{q_s}{q_0}\frac{\partial\Phi_1}{\partial X}$, etc.

The calculation for the rigid aerofoil to give $\Phi_1$, $\Phi_2$, $\Phi_3$ having been completed, it is only necessary to obtain in addition network solutions for a small aerofoil extending from $X = 0{\cdot}6$ to $X = 1$ to give $\Phi_{1\beta}$ and $\Phi_{2\beta}$. For this small aerofoil the angle corresponding to the semi-wedge angle $w$ of the complete aerofoil is $-1{\cdot}14496$ when $t/c = 0{\cdot}05$ and $-1{\cdot}71566$ when $t/c = 0{\cdot}075$. The same spacing for the network is used as before, yielding values of $\Phi$ at $X = 0{\cdot}7$, $0{\cdot}8$, $0{\cdot}9$, $1{\cdot}0$ ($X_f = 0{\cdot}1$, $0{\cdot}2$, $0{\cdot}3$, $0{\cdot}4$). In this case the $\Phi$ values obtained from the network solution are represented as a quadratic for the purpose of determining $\partial\Phi/\partial X$.

5. *Results for Aerofoil with Flap.*—The coefficient of $\beta$ in the lift distribution is plotted in Fig. 13, together with the exact values associated with $\partial\Phi_{1\beta}/\partial X = -\tan\mu_s \dfrac{q_s}{q_1}$ (for $X = 0{\cdot}6$ to 1). The variation of the inphase component $R$ of the lift distribution with frequency is so small that it cannot be shown in the diagram. For a four-point network solution, the agreement between the exact and the estimated values of $\dfrac{l(\mathrm{X})}{\rho_0 q_0^{\,2}\beta}$ is very satisfactory.

The additional mid-chord derivatives for an aerofoil with flap are given in Table 3; and they are plotted against $\lambda_0$ in Fig. 14, together with values for a flat plate with flap calculated from approximate formulae given in Ref. 5.

In Table 4 the results obtained here for $\lambda_0$ tending to 0 are compared with the limiting values of the leading-edge derivatives given by Temple and Jahn's formulae* for a thin aerofoil with flap (Ref. 2).

For the purpose of comparison, the leading-edge derivatives for $\lambda_0$ tending to 0 calculated for the 5 per cent and the $7{\cdot}5$ per cent thick rigid aerofoils are given in Table 5, together with the corresponding values obtained from Temple and Jahn's formulae for a thin aerofoil.

A comparison of Tables 4 and 5 shows that the derivatives for an aerofoil with flap vary with thickness in much the same way as those of a rigid aerofoil.

6. *Concluding Remarks.*—The results given here for a rigid aerofoil confirm the conclusions given in Ref. 1 that thickness has a marked effect on the aerodynamic derivatives; and it is shown, moreover, that this effect ceases to be linear as $t/c$ increases.

It is difficult to judge from results so far available how nearly theory agrees with experiment. Fig. 7 shows, however, that, for mid-chord axis position, the present theory agrees with experiment in giving an increase of $-m_{\dot{\alpha}}$ as $M_0$ decreases, whereas flat plate theory gives a decrease in $-m_{\dot{\alpha}}$ as $M_0$ decreases.

The theory developed in Ref. 1 neglects the effect of the shock wave at the leading edge, and the effect of the boundary layer. The latter effect would result in a falling off of lift towards the trailing edge of the aerofoil (Ref. 4). In order to get some idea of the magnitude of this effect, the value of the mid-chord stiffness coefficient $-m_\alpha$ for the $7{\cdot}5$ per cent thick aerofoil at $M_0 = 1{\cdot}5$ is calculated when the lift is neglected beyond a certain value of $X$. It is thus found that the experimental value of $-m_\alpha$ ($-0{\cdot}254$) is arrived at by neglecting the lift beyond a point estimated to be $X = 0{\cdot}748$. The value of the damping coefficient $-m_{\dot{\alpha}}$ obtained by neglecting the lift beyond the point $X = 0{\cdot}748$ is found to be $0{\cdot}173$, which agrees more nearly with the experimental value of $0{\cdot}28$ than the value of $0{\cdot}070$ corresponding to the normal lift distribution of the present theory. The effect due to boundary layer would thus appear to be in the right direction.

As already indicated, however, the effect of axis position on the experimental values needs further investigation.

---

* If $x_0$ (denoted here by $\bar{h}$) is put equal to 0 in the expressions of Ref. 5, the resulting leading-edge derivatives for $\lambda_0$ tending to 0 agree with those given by Temple and Jahn's simple formulae.

In view of the marked effects of the boundary layer near the trailing edge, no accuracy can be claimed for the calculated values of the derivatives for an aerofoil with flap. The calculation was carried through for one value of $M_0$ (1·7) merely to indicate whether the scheme of computation used for a rigid aerofoil could be applied satisfactorily to an aerofoil carrying a flap. The results obtained appear to be of the right order, and suggest that reliable values could be obtained if a finer network were used and the present theory were modified to allow for the effect of the boundary layer.

## REFERENCES


| *No.* | *Author* | *Title, etc.* |
|---|---|---|
| 1 | W. P. Jones and S. W. Skan .. | Aerodynamic Forces on Biconvex Aerofoils Oscillating in a Supersonic Airstream. See first part of R. & M. 2749. May, 1950. |
| 2 | G. Temple and H. A. Jahn .. | Flutter at Supersonic Speeds: Derivative Coefficients for a thin Aerofoil at Zero Incidence. R. & M. 2140. April, 1945. |
| 3 | J. B. Bratt and A. Chinneck .. | Measurements of Mid-Chord Pitching Moment Derivatives at High Speeds. R. & M. 2680. June, 1947. |
| 4 | D. Beastall and R. J. Pallant .. | Wind Tunnel Tests on Two-dimensional Supersonic Aerofoils at $M$=1·86 and $M$ = 2·48. R. & M. 2800. July, 1950. |
| 5 | V. Huckel and B. J. Durling .. | Tables of Wing-Aileron Coefficients of Oscillating Air Forces for Two-dimensional Supersonic Flow. N.A.C.A. Tech. Note 2055. March, 1950. |


## TABLE 1

*Mid-chord Derivatives for Biconvex Aerofoil* ($t = 0{\cdot}05c$)

| $M_0$ | $\lambda_0$ | $l_\alpha$ | $l_{\dot\alpha}$ | $l_z$ | $l_{\dot z}$ | $-m_\alpha$ | $-m_{\dot\alpha}$ | $-m_z$ | $-m_{\dot z}$ |
|---|---|---|---|---|---|---|---|---|---|
| 2·0 | 0 | 1·168 | —0·334 | 0 | 1·176 | —0·048 | 0·062 | 0 | —0·061 |
| | 0·25 | 1·150 | —0·370 | 0·018 | 1·168 | —0·052 | 0·054 | 0·002 | —0·062 |
| | 0·5 | 1·102 | —0·340 | 0·067 | 1·133 | —0·061 | 0·061 | 0·009 | —0·070 |
| | 0·75 | 1·031 | —0·299 | 0·135 | 1·082 | —0·073 | 0·072 | 0·015 | —0·081 |
| 1·7 | 0 | 1·472 | —0·595 | 0 | 1·493 | —0·057 | 0·060 | 0 | —0·074 |
| 1·5 | 0 | 1·813 | —1·086 | 0 | 1·848 | —0·083 | 0·054 | 0 | —0·110 |
| | 0·25 | 1·731 | —1·114 | 0·065 | 1·778 | —0·097 | 0·049 | 0·007 | —0·125 |
| | 0·5 | 1·513 | —0·907 | 0·221 | 1·597 | —0·131 | 0·097 | 0·017 | —0·160 |
| | 0·75 | 1·260 | —0·633 | 0·378 | 1·362 | —0·158 | 0·156 | 0·008 | —0·198 |
| 1·4 | 0 | 2·083 | —1·712 | 0 | 2·135 | —0·108 | 0·038 | 0 | —0·145 |
| | 0·05 | 2·075 | —1·886 | 0·004 | 2·128 | —0·109 | 0·004 | 0 | —0·146 |
| | 0·15 | 2·022 | —1·822 | 0·040 | 2·081 | —0·118 | 0·018 | 0·004 | —0·155 |
| | 0·25 | 1·919 | —1·702 | 0·105 | 1·990 | —0·135 | 0·046 | 0·009 | —0·172 |
| | 0·5 | 1·539 | —1·222 | 0·322 | 1·639 | —0·184 | 0·153 | 0·012 | —0·233 |
| | 0·75 | 1·184 | —0·651 | 0·456 | 1·271 | —0·197 | 0·263 | —0·034 | —0·272 |

## TABLE 2

*Mid-chord Derivatives for Biconvex Aerofoil* ($t = 0{\cdot}075c$)

| $M_0$ | $\lambda_0$ | $l_\alpha$ | $l_{\dot\alpha}$ | $l_z$ | $l_{\dot z}$ | $-m_\alpha$ | $-m_{\dot\alpha}$ | $-m_z$ | $-m_{\dot z}$ |
|---|---|---|---|---|---|---|---|---|---|
| 2·0 | 0 | 1·185 | −0·420 | 0 | 1·213 | −0·072 | 0·062 | 0 | −0·088 |
| | 0·25 | 1·162 | −0·472 | 0·022 | 1·198 | −0·076 | 0·050 | 0·003 | −0·091 |
| | 0·5 | 1·100 | −0·432 | 0·082 | 1·154 | −0·087 | 0·060 | 0·010 | −0·101 |
| | 0·75 | 1·011 | −0·373 | 0·164 | 1·088 | −0·102 | 0·074 | 0·016 | −0·115 |
| 1·7 | 0 | 1·485 | −0·733 | 0 | 1·531 | −0·087 | 0·065 | 0 | −0·114 |
| | 0·25 | 1·436 | −0·787 | 0·042 | 1·493 | −0·096 | 0·054 | 0·004 | −0·122 |
| | 0·5 | 1·304 | −0·687 | 0·152 | 1·389 | −0·117 | 0·078 | 0·014 | −0·143 |
| | 0·75 | 1·132 | −0·536 | 0·283 | 1·243 | −0·139 | 0·112 | 0·015 | −0·169 |
| 1·5 | 0 | 1·826 | −1·410 | 0 | 1·906 | −0·130 | 0·070 | 0 | −0·174 |
| | 0·25 | 1·690 | −1·488 | 0·090 | 1·786 | −0·151 | 0·067 | 0·007 | −0·197 |
| | 0·5 | 1·366 | −1·095 | 0·284 | 1·487 | −0·191 | 0·153 | 0·008 | −0·247 |
| | 0·75 | 1·056 | −0·619 | 0·414 | 1·158 | −0·199 | 0·241 | −0·032 | −0·281 |

## TABLE 3

*Mid-chord Derivatives for Biconvex Aerofoil with Flap.* $M_0 = 1{\cdot}7$

| $t/c$ | $\lambda_0$ | $l_\beta$ | $l_{\dot\beta}$ | $-m_\beta$ | $-m_{\dot\beta}$ | $-h_z$ | $-h_{\dot z}$ |
|---|---|---|---|---|---|---|---|
| 0·075 | 0 | 0·468 | 0·0362 | 0·136 | 0·0128 | 0 | 0·0866 |
| | 0·25 | 0·467 | 0·0336 | 0·135 | 0·0119 | 0·0047 | 0·0807 |
| | 0·5 | 0·466 | 0·0337 | 0·135 | 0·0119 | 0·0155 | 0·0648 |
| | 0·75 | 0·465 | 0·0340 | 0·135 | 0·0120 | 0·0240 | 0·0444 |
| 0·05 | 0 | 0·501 | 0·0420 | 0·147 | 0·0151 | 0 | 0·0952 |

| $t/c$ | $\lambda_0$ | $-h_\alpha$ | $-h_{\dot\alpha}$ | $-h_\beta$ | $-h_{\dot\beta}$ |
|---|---|---|---|---|---|
| 0·075 | 0 | 0·0896 | −0·0382 | 0·0896 | 0·00922 |
| | 0·25 | 0·0835 | −0·0467 | 0·0886 | 0·00856 |
| | 0·5 | 0·0658 | −0·0294 | 0·0884 | 0·00858 |
| | 0·75 | 0·0457 | −0·0046 | 0·0882 | 0·00863 |
| 0·05 | 0 | 0·0978 | −0·0282 | 0·0978 | 0·01087 |

## TABLE 4

*Leading-edge Derivatives when $\lambda_0 \to 0$ for Biconvex Aerofoils with Flap, Compared with Corresponding Limiting Values for Thin Aerofoil with Flap*

| Derivative | Temple and Jahn's Formula for Thin Aerofoil (Reference 2) | Value Given by Formula | Value given by Network Solution for Biconvex Aerofoil | |
|---|---|---|---|---|
| | | | $t = 0{\cdot}05c$ | $t = 0{\cdot}075c$ |
| $\bar{l}_\beta$ | $2E \tan \mu$ .. .. .. .. | 0·582 | 0·501 | 0·468 |
| $\bar{l}_{\dot{\beta}}$ | $E^2 \tan \mu\,(1 - \tan^2 \mu)$ .. .. | 0·055 | 0·042 | 0·036 |
| $-\bar{m}_\beta$ | $E\,(2 - E) \tan \mu$ .. .. .. | 0·466 | 0·398 | 0·369 |
| $-\bar{m}_{\dot{\beta}}$ | $E^2\left(1 - \frac{E}{3}\right) \tan \mu\,(1 - \tan^2 \mu)$ .. | 0·047 | 0·036 | 0·031 |
| $-\bar{h}_z$ | 0 .. .. .. .. .. | 0 | 0 | 0 |
| $-\bar{h}_{\dot{z}}$ | $E^2 \tan \mu$ .. .. .. .. | 0·116 | 0·095 | 0·087 |
| $-\bar{h}_\alpha$ | $E^2 \tan \mu$ .. .. .. .. | 0·116 | 0·098 | 0·090 |
| $-\bar{h}_{\dot{\alpha}}$ | $E^2\left(1 - \frac{E}{3}\right) \tan \mu\,(1 - \tan^2 \mu)$ .. | 0·047 | 0·019 | 0·005 |
| $-\bar{h}_{\dot{\beta}}$ | $E^2 \tan \mu$ .. .. .. .. | 0·116 | 0·098 | 0·090 |
| $-\bar{h}_{\dot{\beta}}$ | $\frac{2}{3} E^3 \tan \mu\,(1 - \tan^2 \mu)$ .. .. | 0·015 | 0·011 | 0·009 |

Bars are used here to distinguish the leading-edge derivatives from the mid-chord derivatives of Table 3.
$\mu$ = Mach angle. $\tan \mu = 0{\cdot}7274$ for $M_0 = 1{\cdot}7$.
$E$ = ratio of flap chord to total chord = 0·4.

## TABLE 5

*Leading-edge Derivatives when $\lambda_0 \to 0$ for Biconvex Aerofoils, Compared with Corresponding Limiting Values for Thin Aerofoil*

| Derivative | Temple and Jahn's Formula for Thin Aerofoil | Value given by Formula | Value given by Network Solution for Biconvex Aerofoil | |
|---|---|---|---|---|
| | | | $t = 0{\cdot}05c$ | $t = 0{\cdot}075c$ |
| $\bar{l}_z$ | 0 .. .. .. .. .. | 0 | 0 | 0 |
| $\bar{l}_{\dot{z}}$ | $2 \tan \mu$ .. .. .. .. .. | 1·455 | 1·493 | 1·531 |
| $\bar{l}_\alpha$ | $2 \tan \mu$ .. .. .. .. | 1·455 | 1·472 | 1·485 |
| $\bar{l}_{\dot{\alpha}}$ | $\tan \mu\,(1 - \tan^2 \mu)$ .. .. .. | 0·343 | 0·152 | 0·032 |
| $-\bar{m}_z$ | 0 .. .. .. .. .. | 0 | 0 | 0 |
| $-\bar{m}_{\dot{z}}$ | $\tan \mu$ .. .. .. .. .. | 0·727 | 0·673 | 0·652 |
| $-\bar{m}_\alpha$ | $\tan \mu$ .. .. .. .. .. | 0·727 | 0·680 | 0·655 |
| $-\bar{m}_{\dot{\alpha}}$ | $\frac{2}{3} \tan \mu\,(1 - \tan^2 \mu)$ .. .. | 0·228 | 0·099 | 0·024 |

Bars are used here to distinguish the leading-edge derivatives from the mid-chord derivatives of Tables 1 and 2.
$\tan \mu = 0{\cdot}7274$ for $M_0 = 1{\cdot}7$.

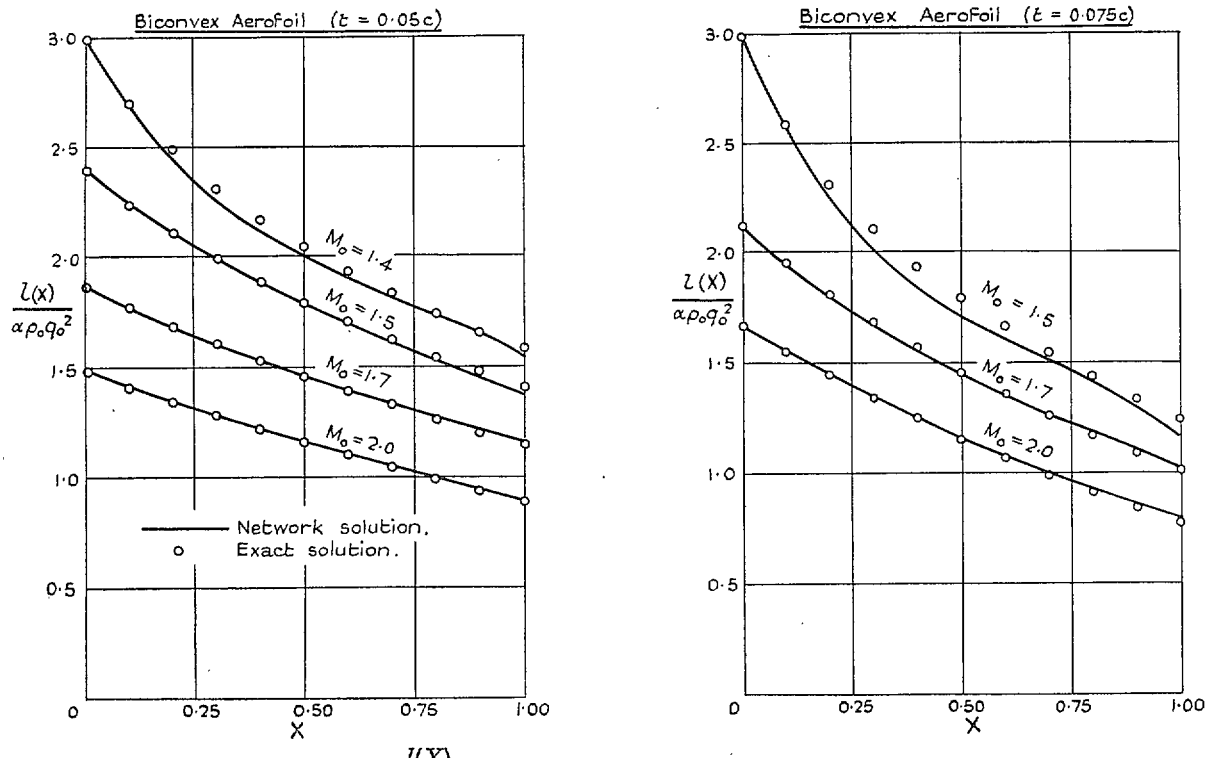


FIG. 1. Values of $\frac{l(X)}{\alpha\rho_0 q_0^2}$ ($\lambda_0 = 0$) for oscillations about the mid-chord axis.

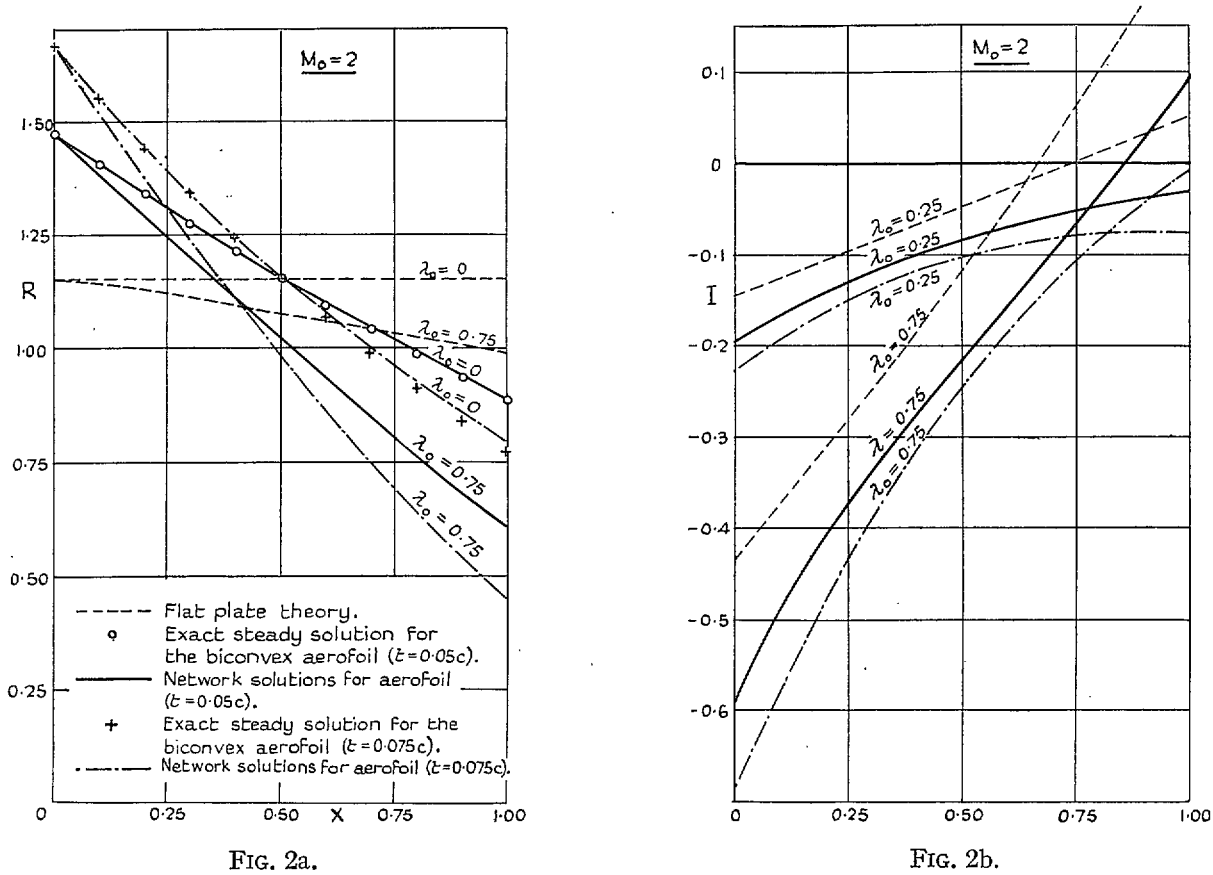


FIG. 2a. FIG. 2b.

FIGS. 2a and 2b. Values of $\frac{l(X)}{\alpha\rho_0 q_0^2}$ ($\equiv R + iI$) for oscillations about the mid-chord axis.

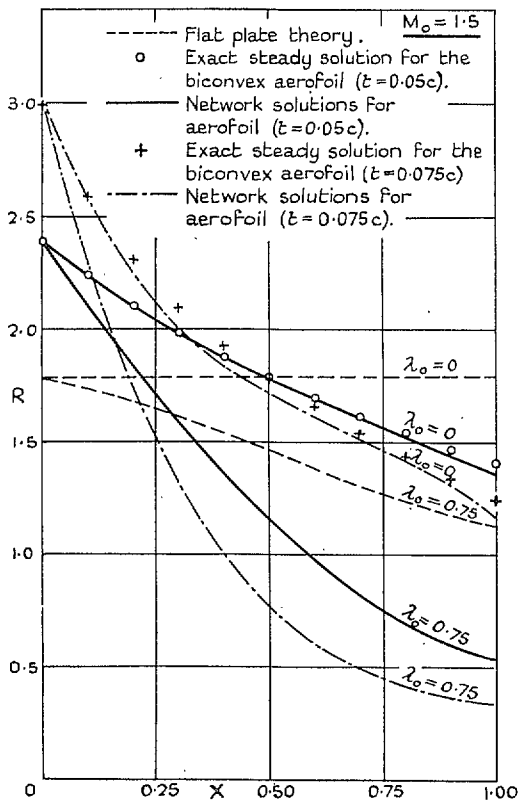


FIG. 3a.

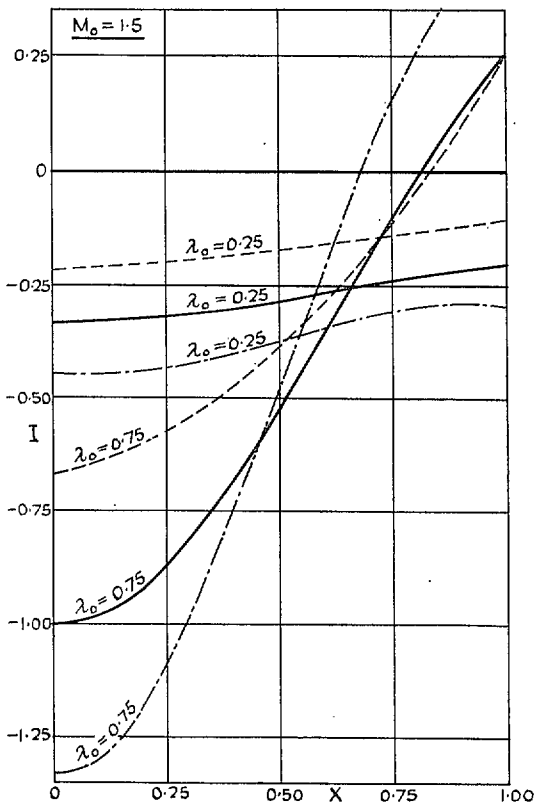


FIG. 3b.

FIGS. 3a and 3b. Values of $\frac{l(X)}{\alpha\rho_0 q_0^2}$ $(\equiv R + iI)$ for oscillations about the mid-chord axis.

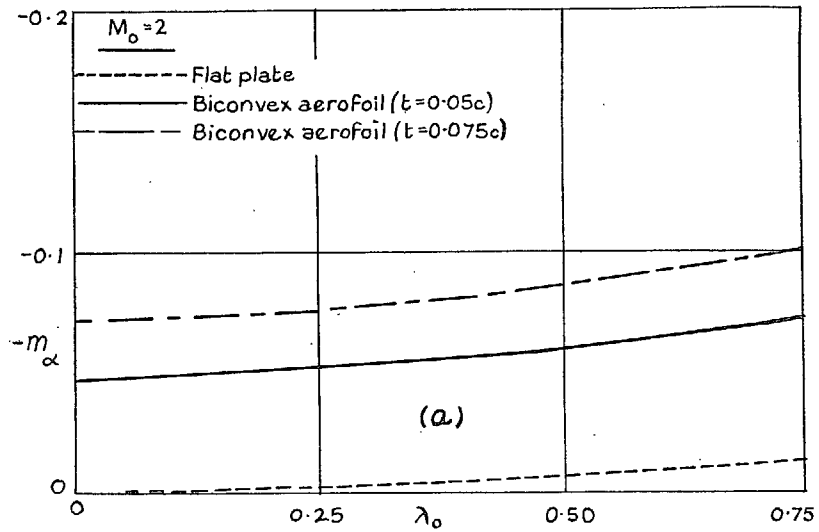


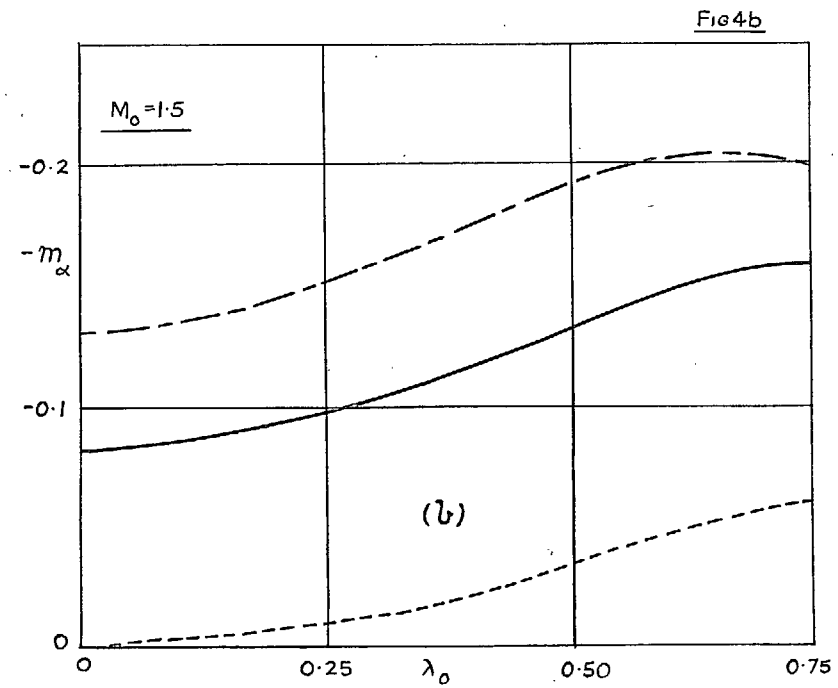


FIGS. 4a and 4b. Values of the aerodynamic stiffness coefficient for pitching oscillations about the mid-chord axis.

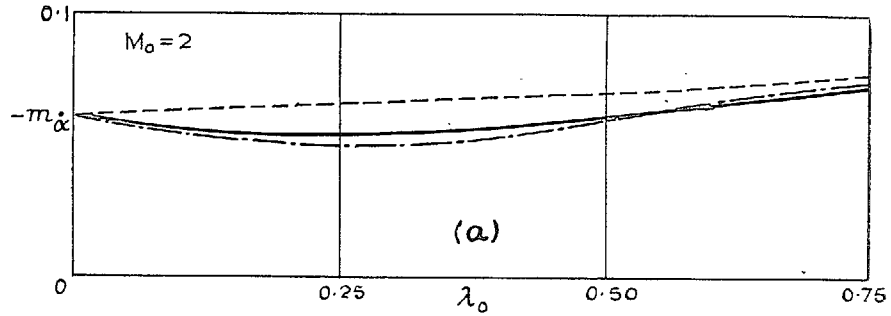


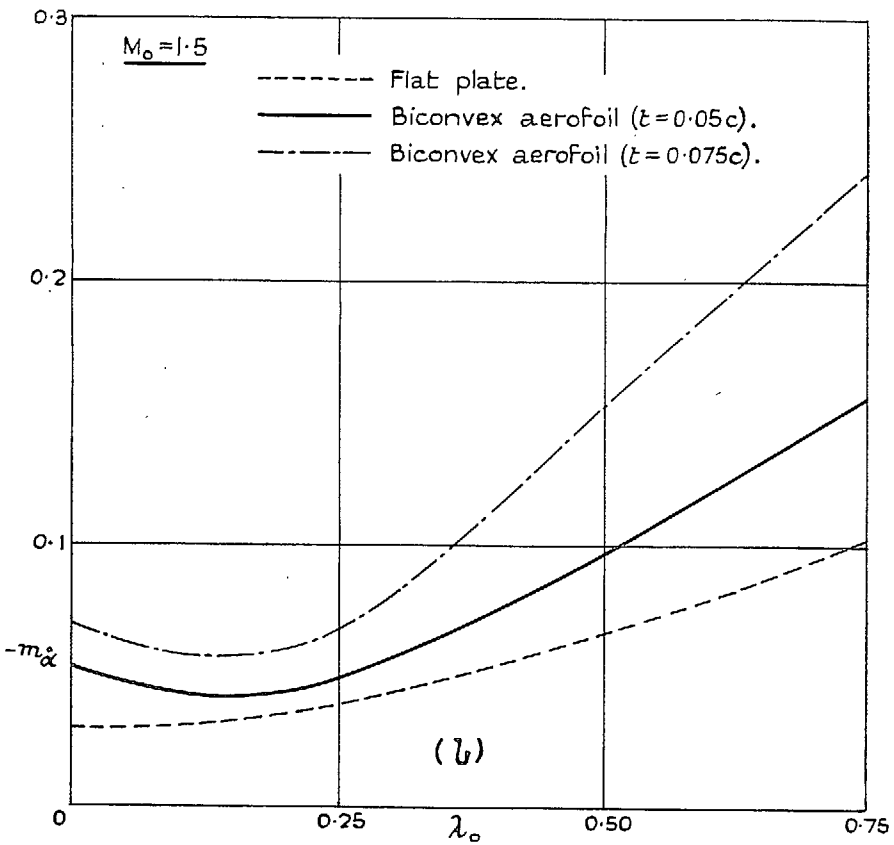


FIGS. 5a and 5b. Values of the aerodynamic damping coefficient for pitching oscillations about the mid-chord axis.

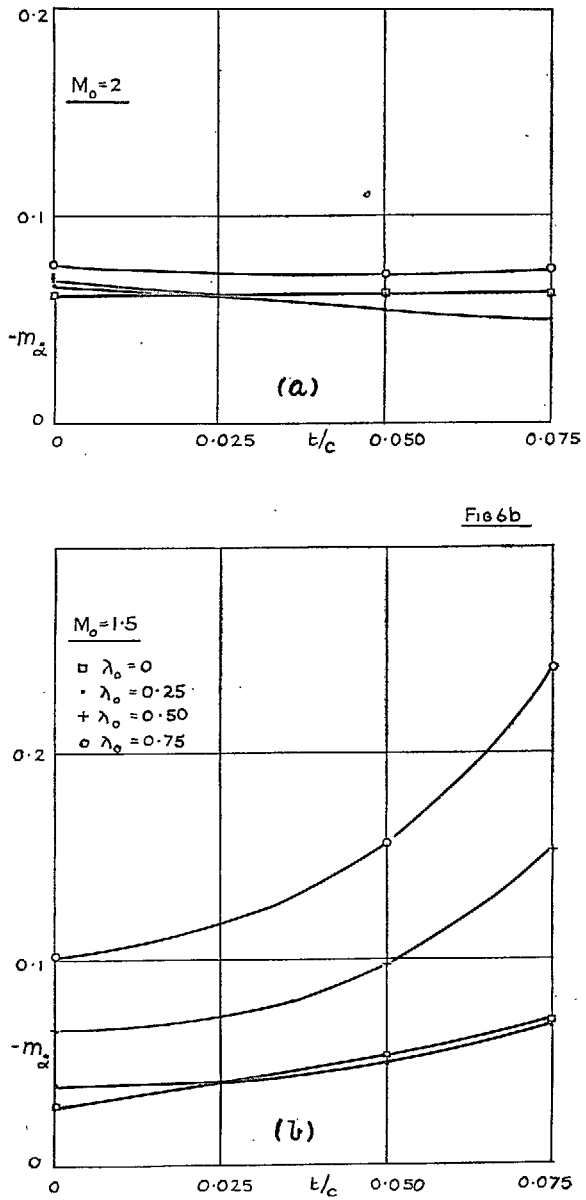


FIGS. 6a and 6b. Variation of the coefficient — $m_{\dot{\alpha}}$ with thickness (mid-chord axis).

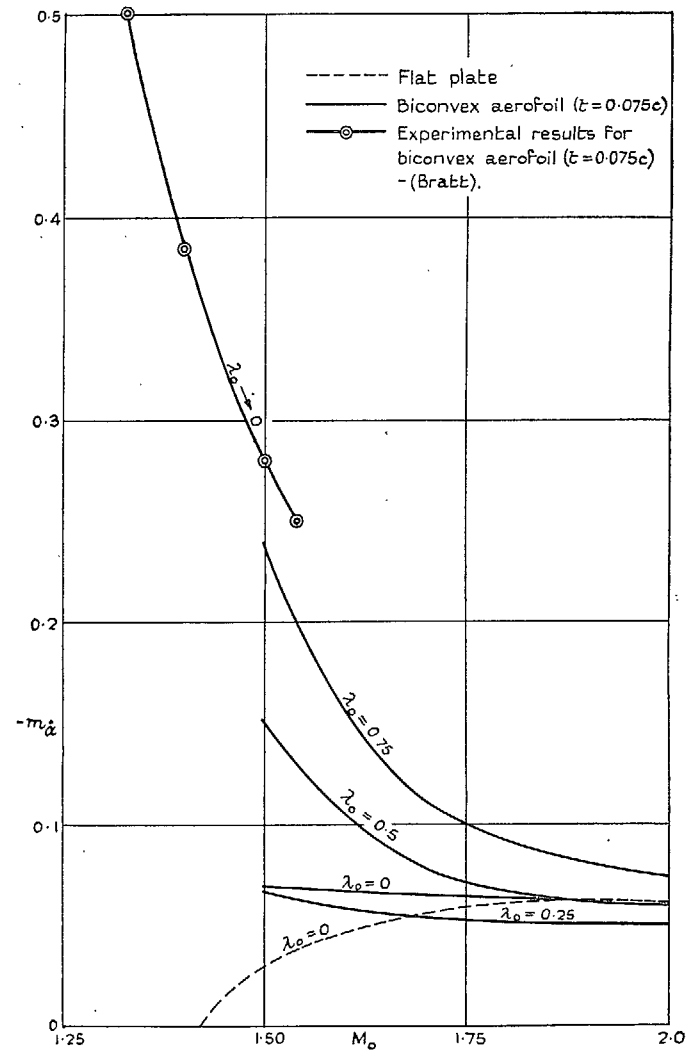


FIG. 7. Variation of the coefficient — $m_{\dot{\alpha}}$ with Mach number (mid-chord axis).

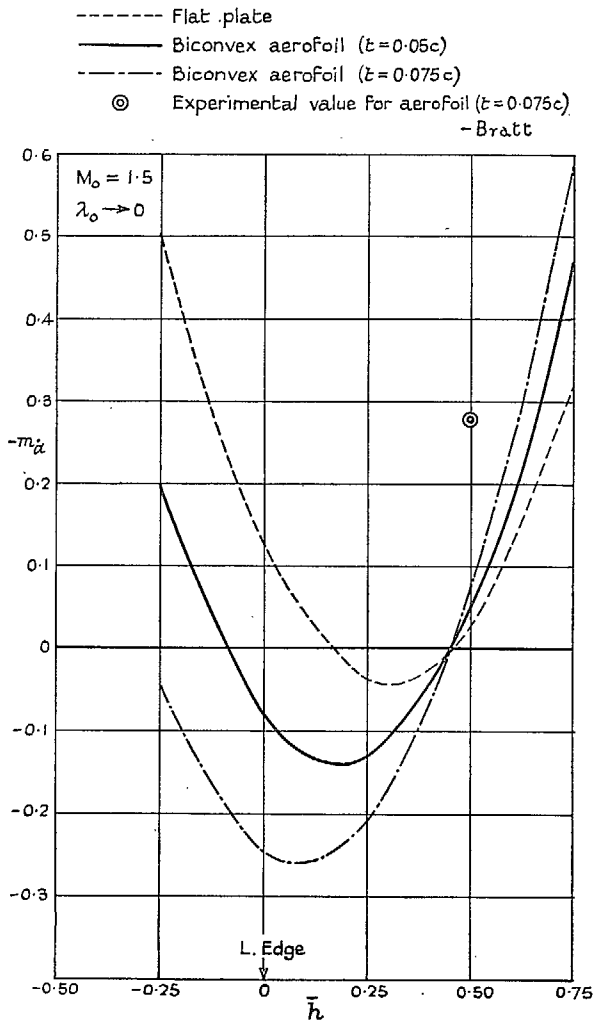


FIG. 8. Variation of the coefficient $-m_{\dot{\alpha}}$ with axis position.

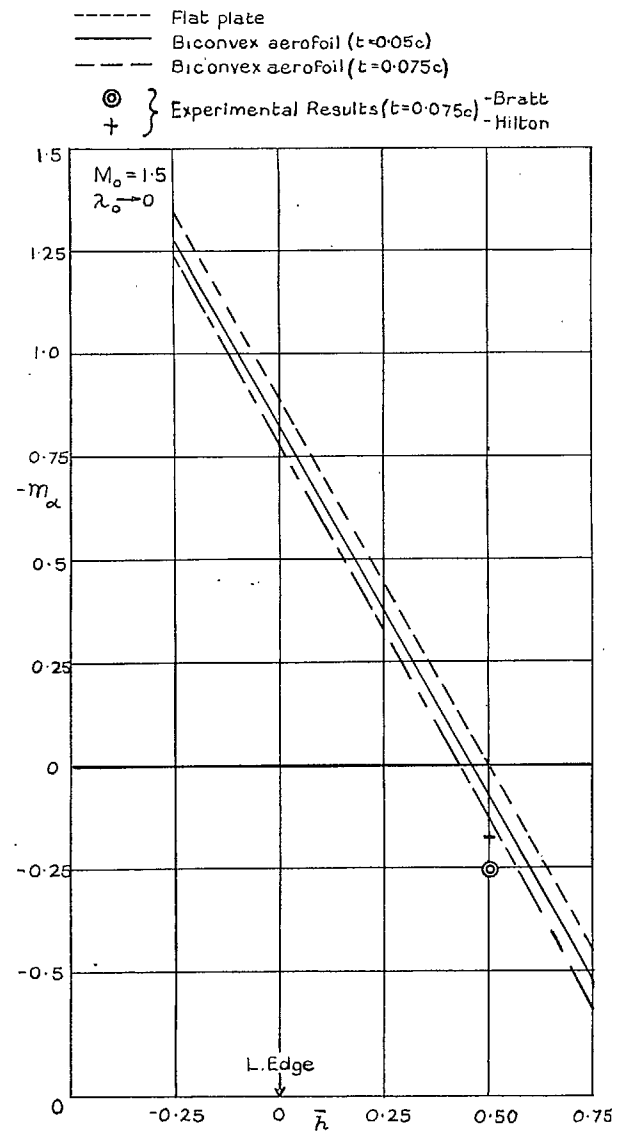


FIG. 9. Variation of the coefficient $-m_{\alpha}$ with axis position.

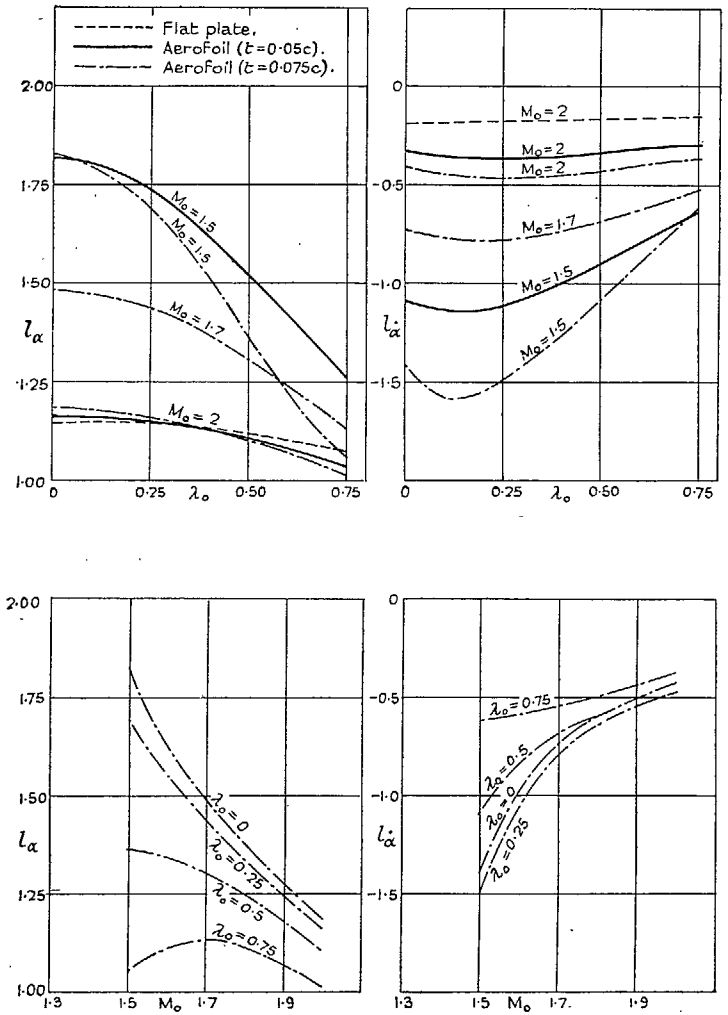


FIG. 10. Values of the coefficients $l_a$ and $l_{\dot a}$ (mid-chord axis).

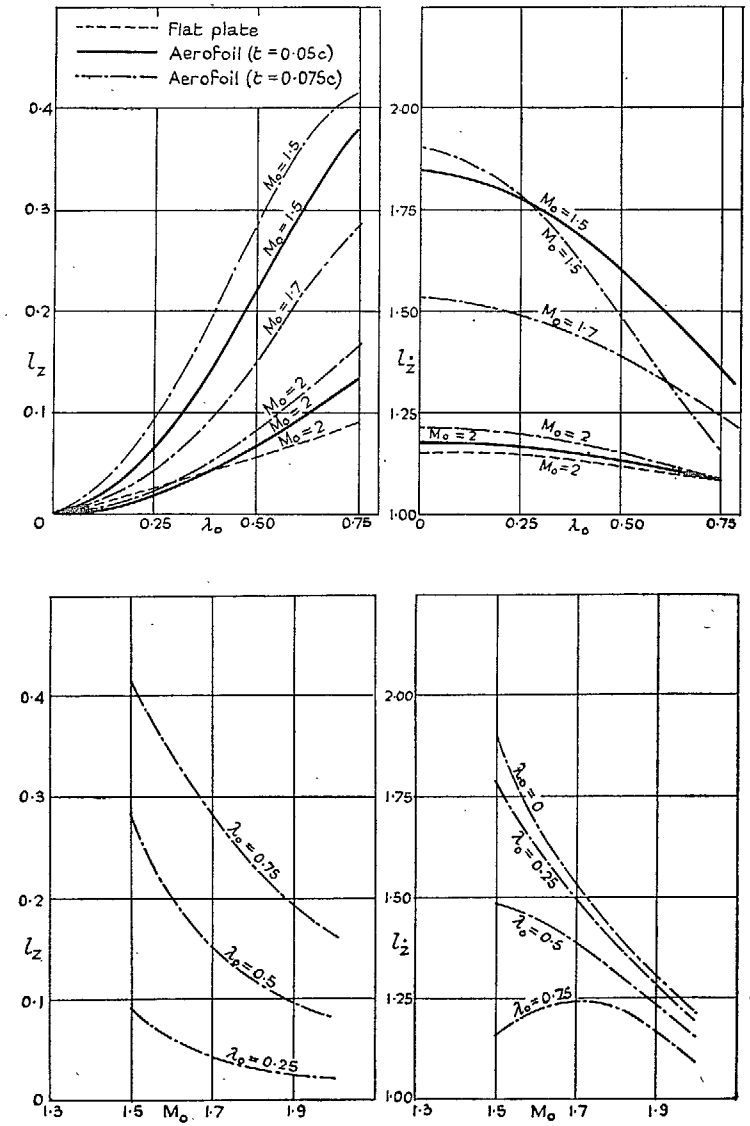


FIG. 11. Values of coefficients $l_z$ and $l_{\dot z}$ (mid-chord axis).

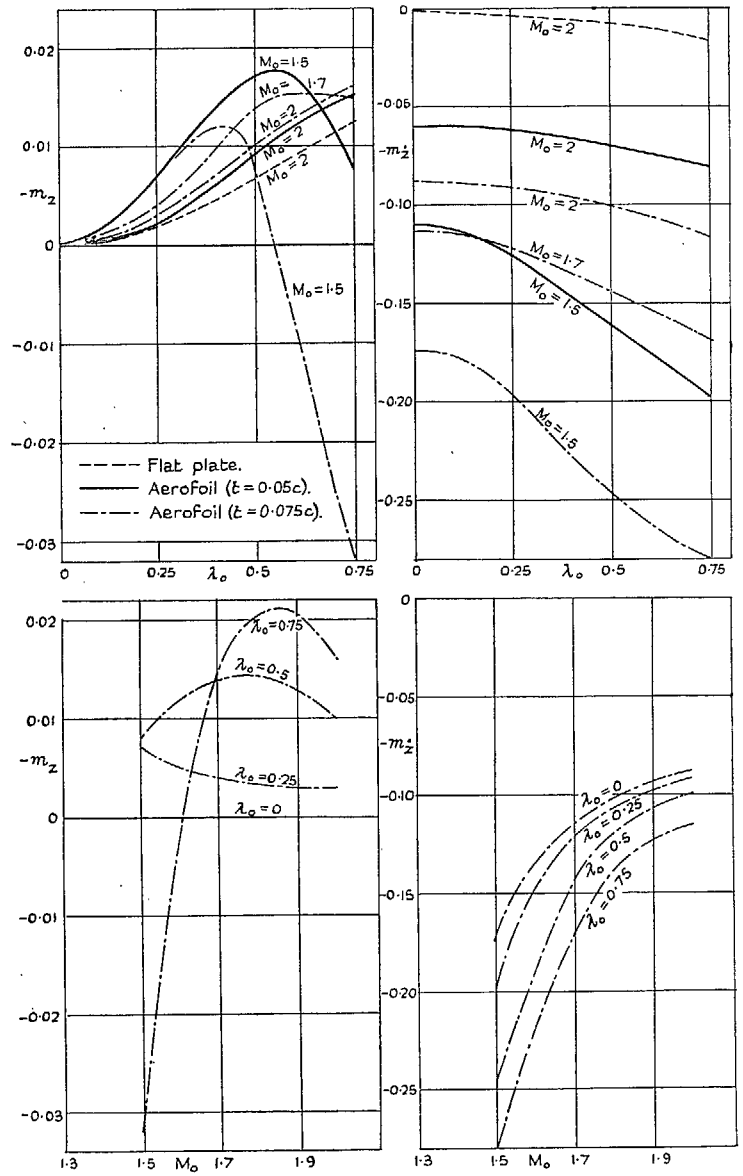


FIG. 12. Values of the coefficients $-m_z$ and $-m_z$ (mid-chord axis).

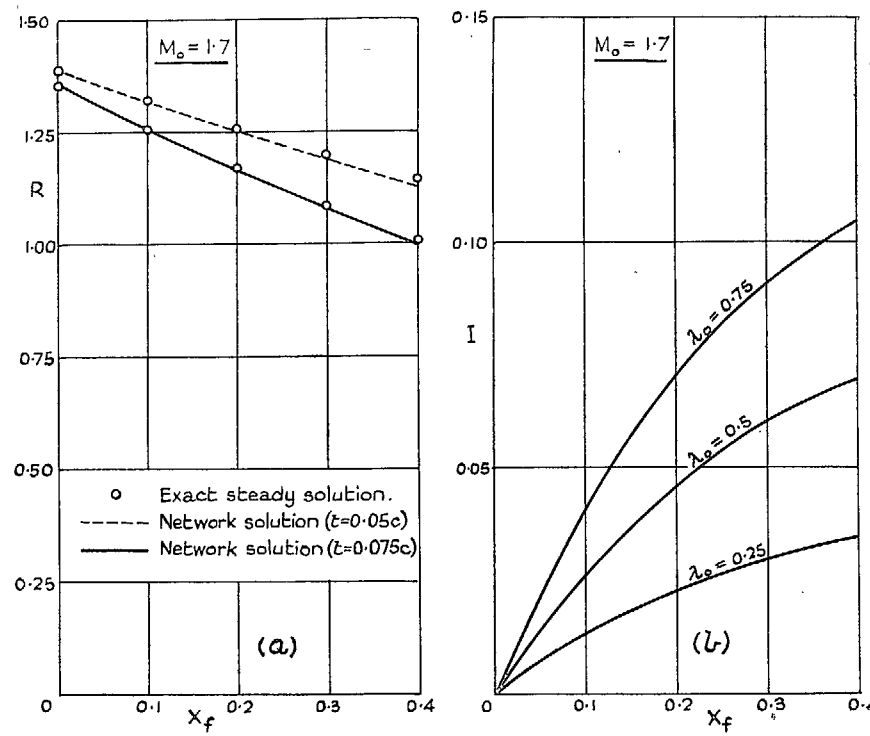


FIGS. 13a and 13b. Values of $\frac{l(X)}{\rho_0 q_0^2 \beta} (\equiv R + iI)$ for oscillations of flap about the hinge.

(52568) Wt. 15/680 K.9 4/53 Hw.



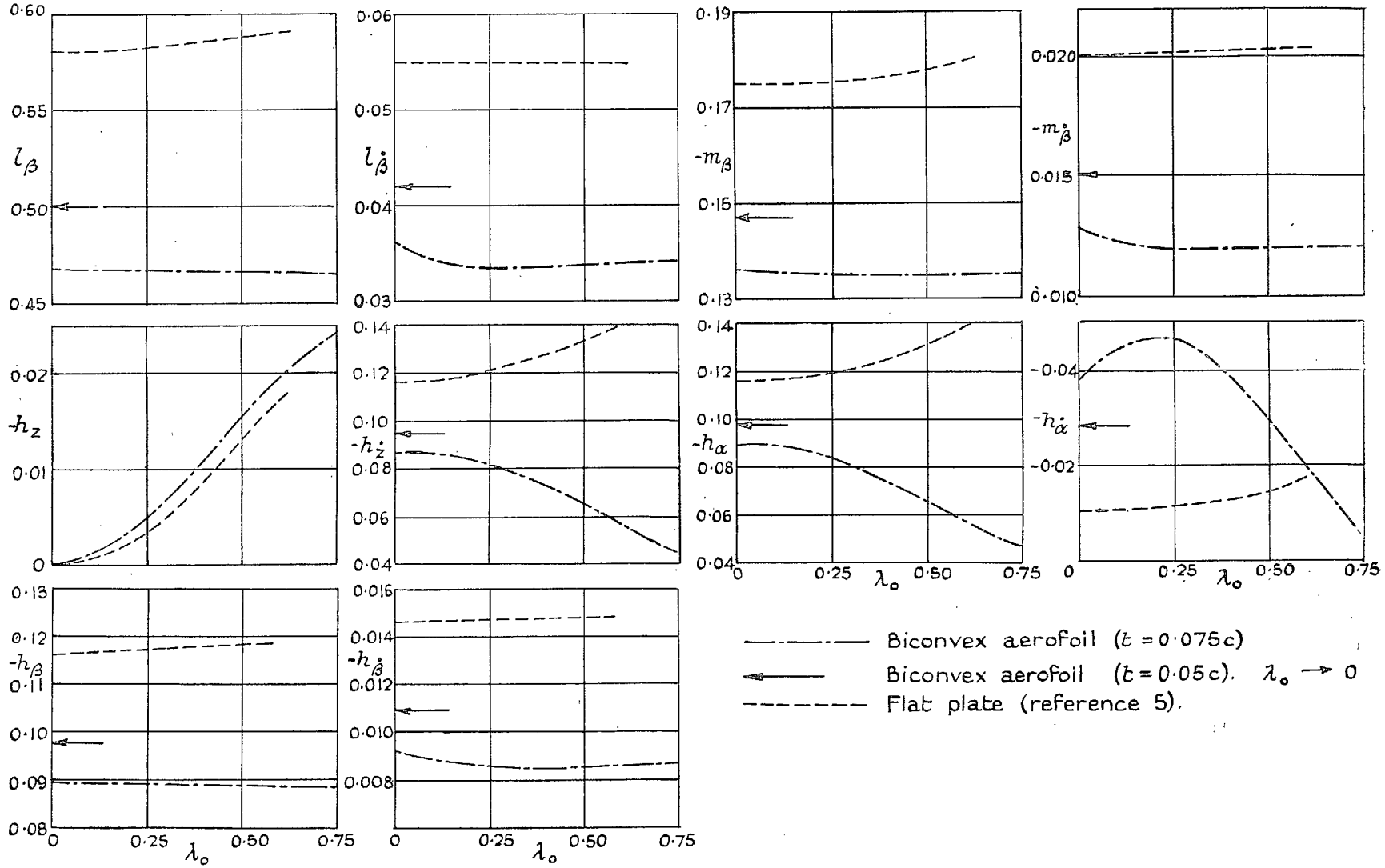


FIG. 14. Mid-chord derivatives for biconvex aerofoil with flap. $M_0 = 1{\cdot}7$.

PRINTED IN GREAT BRITAIN

# Publications of the Aeronautical Research Council

## ANNUAL TECHNICAL REPORTS OF THE AERONAUTICAL RESEARCH COUNCIL (BOUND VOLUMES)

1936 Vol. I. Aerodynamics General, Performance, Airscrews, Flutter and Spinning. 40*s*. (40*s*. 9*d*.)
Vol. II. Stability and Control, Structures, Seaplanes, Engines, etc. 50*s*. (50*s*. 10*d*.)

1937 Vol. I. Aerodynamics General, Performance, Airscrews. Flutter and Spinning. 40*s*. (40*s*. 10*d*.)
Vol. II. Stability and Control, Structures, Seaplanes, Engines, etc. 60*s*. (61*s*.)

1938 Vol. I. Aerodynamics General, Performance, Airscrews. 50*s*. (51*s*.)
Vol. II. Stability and Control, Flutter, Structures, Seaplanes, Wind Tunnels, Materials. 30*s*. (30*s*. 9*d*.)

1939 Vol. I. Aerodynamics General, Performance, Airscrews, Engines. 50*s*. (50*s*. 11*d*.)
Vol. II. Stability and Control, Flutter and Vibration, Instruments, Structures, Seaplanes, etc. 63*s*. (64*s*. 2*d*.)

1940 Aero and Hydrodynamics, Aerofoils, Airscrews, Engines, Flutter, Icing, Stability and Control, Structures, and a miscellaneous section. 50*s*. (51*s*.)

1941 Aero and Hydrodynamics, Aerofoils, Airscrews, Engines, Flutter, Stability and Control, Structures. 63*s*. (64*s*. 2*d*.)

1942 Vol. I. Aero and Hydrodynamics, Aerofoils, Airscrews, Engines. 75*s*. (76*s*. 3*d*.)
Vol. II. Noise, Parachutes, Stability and Control, Structures, Vibration, Wind Tunnels. 47*s*. 6*d*. (48*s*. 5*d*.)

1943 Vol. I. (*In the press*.)
Vol. II. (*In the press*.)

## ANNUAL REPORTS OF THE AERONAUTICAL RESEARCH COUNCIL—

| | | | |
|---|---|---|---|
| 1933–34 | 1*s*. 6*d*. (1*s*. 8*d*.) | 1937 | 2*s*. (2*s*. 2*d*.) |
| 1934–35 | 1*s*. 6*d*. (1*s*. 8*d*.) | 1938 | 1*s*. 6*d*. (1*s*. 8*d*.) |
| April 1, 1935 to Dec. 31, 1936. | 4*s*. (4*s*. 4*d*.) | 1939–48 | 3*s*. (3*s*. 2*d*.) |

## INDEX TO ALL REPORTS AND MEMORANDA PUBLISHED IN THE ANNUAL TECHNICAL REPORTS, AND SEPARATELY—

April, 1950 - - - - R. & M. No. 2600. 2*s*. 6*d*. (2*s*. 7½*d*.)

## AUTHOR INDEX TO ALL REPORTS AND MEMORANDA OF THE AERONAUTICAL RESEARCH COUNCIL—

1909–1949. R. & M. No. 2570. 15*s*. (15*s*. 3*d*.)

## INDEXES TO THE TECHNICAL REPORTS OF THE AERONAUTICAL RESEARCH COUNCIL—

| | | |
|---|---|---|
| December 1, 1936 — June 30, 1939. | R. & M. No. 1850. | 1*s*. 3*d*. (1*s*. 4½*d*.) |
| July 1, 1939 — June 30, 1945. | R. & M. No. 1950. | 1*s*. (1*s*. 1½*d*.) |
| July 1, 1945 — June 30, 1946. | R. & M. No. 2050. | 1*s*. (1*s*. 1½*d*.) |
| July 1, 1946 — December 31, 1946. | R. & M. No. 2150. | 1*s*. 3*d*. (1*s*. 4½*d*.) |
| January 1, 1947 — June 30, 1947. | R. & M. No. 2250. | 1*s*. 3*d*. (1*s*. 4½*d*.) |
| July, 1951. | R. & M. No. 2350. | 1*s*. 9*d*. (1*s*. 10½*d*.) |

*Prices in brackets include postage.*

Obtainable from

## HER MAJESTY'S STATIONERY OFFICE

York House, Kingsway, London, W.C.2; 423 Oxford Street, London, W.1 (Post Orders: P.O. Box 569, London, S.E.1); 13a Castle Street, Edinburgh 2; 39, King Street, Manchester, 2; 2 Edmund Street, Birmingham 3; 1 St. Andrew's Crescent, Cardiff; Tower Lane, Bristol 1; 80 Chichester Street, Belfast, or through any bookseller